Progress in Natural Science: Materials International 34 (2024) 437–453

HOSTED BY

ELSEVIER

Contents lists available at ScienceDirect

Progress in Natural Science: Materials International

journal homepage: www.elsevier.com/locate/pnsmi

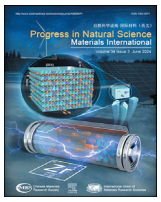

Roles of functionalized nanoparticles in the performance improvement of proton-exchange membranes used in low- and intermediate-temperature hydrogen fuel cells: A review

Abdul Salam, Oksana Zholobko, Xiang-Fa Wu *

Department of Mechanical Engineering, North Dakota State University, Fargo, ND, 58108, USA

ARTICLE INFO

Keywords:
Proton-exchange membrane (PEM)
Proton-exchange membrane fuel cell (PEMFC)
Nanoparticle (NP)
Surface modification
Proton conductivity
Nanocomposite

ABSTRACT

A variety of nanoparticles (NPs) (e.g., SiO_2, TiO_2, CeO_2, Co_3O_4, etc.) and their functionalized counterparts have been intensively investigated for improving the electrochemical and mechanical durability of polymer-based proton-exchange membranes (PEMs) for use in low- and intermediate-temperature fuel cells. This study is to conduct a comprehensive review on the roles of functionalized NPs in the performance enhancement of PEMs including proton conductivity, gas crossover resistance, electrochemical and mechanical durability, etc. A brief historical review of PEM fuel cell (PEMFC) technology is made. Typical types of NPs and their functionalization techniques are retrospected and their roles in the performance improvement of PEMs are compared in detail. Consequently, the opportunities and challenges to develop high-performance functionalized NPs for use in PEMs and PEMFCs are prospected and justified.

1. Introduction

Fast depletion of fossil fuels (e.g., petroleum oils, natural gas, etc.) as well as severe global warming and air/environmental pollution due to massive emissions of greenhouse gases and other toxic pollutants after burning fossil fuels has raised worldwide concerns with the sustainable development of world economy and human society. Substantial efforts have been made to eagerly explore innovative, high-efficiency clean energy conversion and storage technologies to mitigate these global challenging issues. Fuel cell technology first debuted in history over 180 years ago, and it has been considered as a compelling resolution and has captured significant attention due to its high efficiency in electrochemical energy conversion and potential to address these concerns and pave the path to a sustainable, clean, and carbon-neutral future [1]. Fig. 1 illustrates a brief historical progress of fuel cell technologies.

In general, fuel cell is an electrochemical device capable of directly converting the chemical energy stored in fuels (e.g., hydrogen, methanol, ethanol, formic acid, glycols, coal, biomass, etc.) into electrical energy without emission of pollutant gases [2]. Based on the electrolytes used, fuel cells can be categorized into proton-exchange membrane fuel cells (PEMFCs), solid oxide fuel cells (SOFCs), molten carbonate fuel cells (MCFCs), phosphoric acid fuel cells (PAFCs), alkaline fuel cells (AFCs) [3], etc. Among others, PEMFCs have been widely investigated and deployed because of their relatively low fabrication costs, high current and power densities, high energy conversion efficiency, low operating temperature, and fast response time upon demand [4,5]. Depending on the type of fuels used, PEMFCs can be further classified into direct methanol fuel cells (DMFCs) [6], direct ethanol fuel cells (DEFCs) [7], hydrogen-oxygen fuel cells (HOFCs) [8], direct ammonia fuel cells (DAFCs), formic acid fuel cells (FAFCs), etc. Table 1 lists the main characteristics of several common types of fuel cells.

In a single-stack PEMFC system as illustrated in Fig. 2, the membrane electrode assembly (MEA) is its core part, which consists of a proton-exchange membrane (PEM) sandwiched between the electrode layers (anode and cathode) that are composed of the electrocatalyst layers directly contacted with the PEM and the porous gas diffusion layers (GDLs) of typical carbon papers or carbon clothes. The porous GDLs support and protect the electrocatalyst layers, act as the current collectors, and facilitate transport of the reactant gases to the electrocatalyst layers as well as the products from the electrocatalysts. Fuel in the form of hydrogen gas (H_2) or other fuel vapors, e.g., methanol (CH_3OH), ethanol (CH_3CH_2OH), formic acid (CHOOH), etc., are supplied to the porous anode while oxygen (O_2) or air is supplied to the porous cathode. When hydrogen molecules encounter the electrocatalyst layer, typically a layer of platinum (Pt) nanoparticles (NPs), they are oxidized and split into H^+ ions (protons) and electrons. The protons transport through the

* Corresponding author.
E-mail address: Xiangfa.wu@ndsu.edu (X.-F. Wu).

https://doi.org/10.1016/j.pnsc.2024.04.004
Received 10 March 2024; Received in revised form 8 April 2024; Accepted 11 April 2024
Available online 25 April 2024

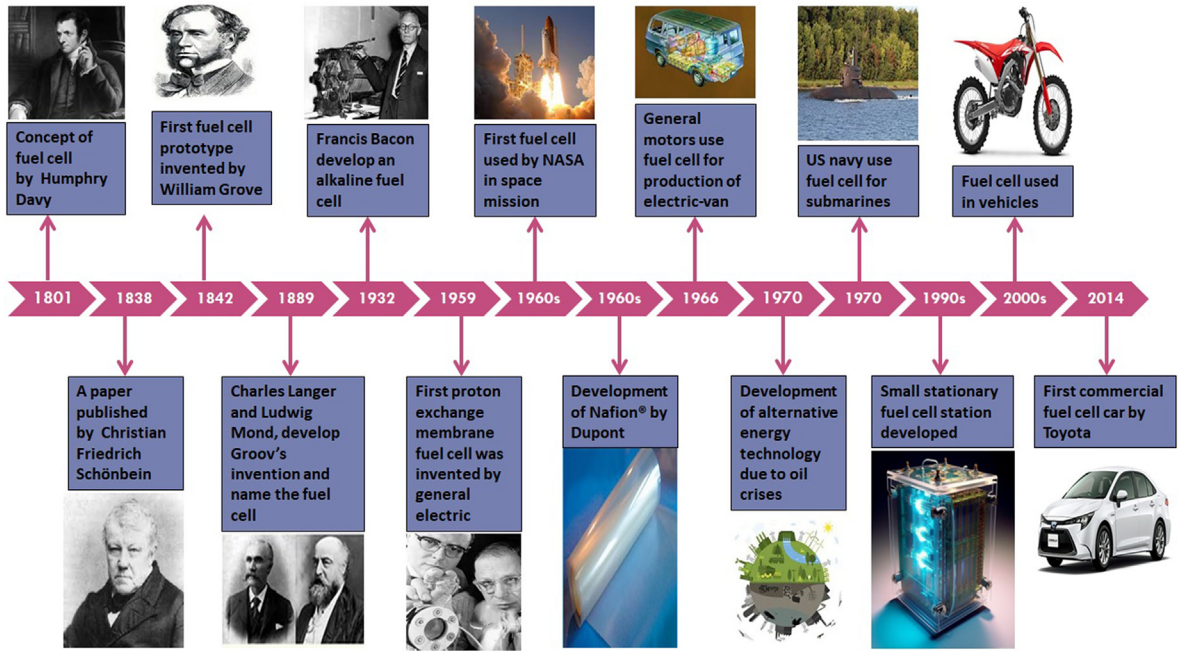

Fig. 1. A brief history of fuel cell technologies: A journey of technological innovations and progress in electrochemical energy conversion [1].

Table 1
Characteristics of several common types of fuel cells [9–11].

Type of fuel cell	Work temperature (°C)	PD ($mWcm^{-2}$)	Electrical efficiency (%)	Applications	Electrolyte
SOFCs	500–1000	250–500	50–60	Stationary powers	Solid, stabilized zirconia ceramic matrix with free oxide ions
PEMFCs	<120	500–2500	40–50	Portable powers, stationary powers, transportation	Polymer membrane
PAFCs	160–220	150–300	40–42	Stationary power, power plants	100 % phosphoric acid (PA) stabilized in alumina-based matrix
MCFCs	600–700	100–300	45–55	Power plants	Li_2CO_3/K_2CO_3 materials stabilized in alumina-based matrix
AFCs	<100	150–400	60	Space vehicles, portable application	KOH solution socked in matrix

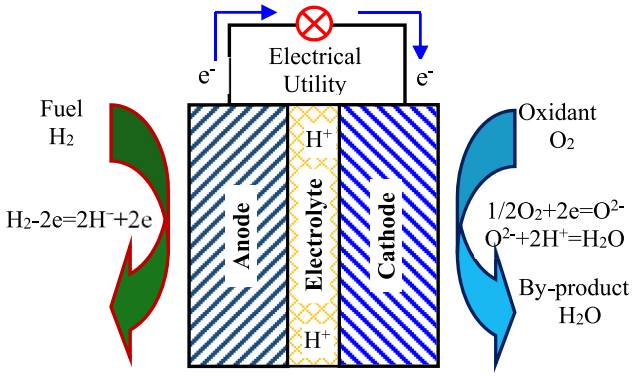

Fig. 2. Schematic diagram of a hydrogen PEMFC.

PEM to the cathode and combine with oxygen anions (O^{2-}), which are reduced from oxygen (O_2) molecules after accepting electrons in the cathode electrocatalyst layer and form water molecules (H_2O) [12]. The electrons flow through the external circuit from the anode towards the cathode to generate the electrical current to power external electrical utilities. The electrochemical reactions taking place at the anode and cathode of a hydrogen PEMFC are.

Anode: Hydrogen-oxidation reaction.

$H_2 \rightarrow 2H^+ + 2e^-$,

Cathode: Oxygen-reduction reaction.

$1/2O_2 + 2e^- \rightarrow O^{2-}$,

$2H^+ + O^{2-} \rightarrow H_2O$.

Overall electrochemical reaction: $H_2 + 1/2O_2 \rightarrow H_2O$.

In a PEMFC, PEM is the key component, through which only protons can pass from the anode toward the cathode. In addition, PEM must be an electrical insulator and blocks the transport of electrons and reactant molecules across the membrane to avoid short-circuiting and fuel leakage of the fuel cell [13]. The key characteristics of an ideal PEM are illustrated in Fig. 3. In principle, ionic (or proton) transport in PEM is a complex physical process involving various types of pathways and mobile protonic species. So far, two main proton-transporting mechanisms are identified, i.e., the Grotthuss (hopping) and vehicle mechanisms. In addition, researchers also reported that interface (or surface) transport could be the third type of proton-transporting mechanism [14,15]. To transport protons, the vehicle mechanism involves the transport of solvated hydronium ions (H_3O^+) in aqueous media. In contrast, the Grotthuss mechanism relies on protons (H^+) jumping from one anion site to another. In this case, breaking and forming bonds involves a higher activation energy compared to the fluidic diffusion of species in the vehicle mechanism. Therefore, at low temperatures and high relative humidity (RH), vehicle mechanism dominates while the Grotthuss mechanism tends to dominate at higher temperatures and low RH. Based on these proton-transporting mechanisms, the total proton conductivity

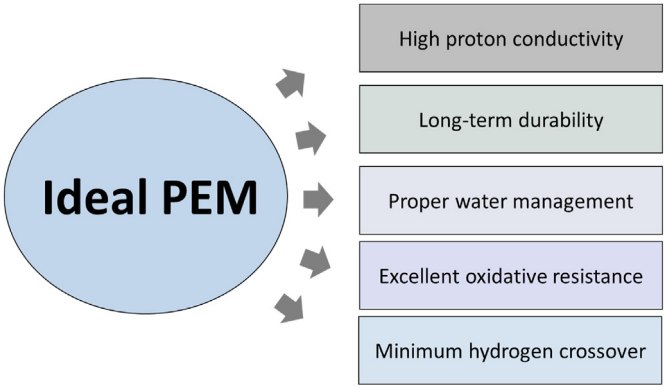

Fig. 3. Essential characteristics of an ideal PEM.

(PC) of a polymer-based PEM relies on the backbone structure of the polymer, its hydrophilicity, the concentration of proton donor-acceptor sites, and the water content.

To date, significant efforts have been devoted to improving the PC and stability of the polymer-based PEMs at higher operating temperatures by incorporating various fillers to form composite membranes. Typically, composite PEMs consist of at least two primary constituents, i.e., the polymer matrix and the organic or inorganic reinforcing phase. The polymer matrix functions to transport protons and enhance the mechanical flexibility of the membrane. The organic or inorganic reinforcing phase improves the water and acid retention capability, PC, as well as the mechanical properties and thermal stability, while suppressing the gas crossover. Synergistically, these contributing factors improve the overall performance and performance durability of PEMs under various operating conditions [16,17].

2. Outstanding issues of PEMFCs and their mitigation

Operating temperature is one of the important process parameters to the overall performance of a fuel cell system. So far, PEMFC technologies have encompassed both low-temperature PEMFCs (LT-PEMFCs) and intermediate-temperature PEMFCs (IT-PEMFCs). Today, perfluorosulfonic acid (PFSA)-based membranes, notably Nafion®, are widely employed as PEMs in LT-PEMFCs. Nafion® demonstrates the exceptional characteristics, e.g., the chemical stability, PC, durability, flexibility, and mechanical strength [18]. However, these properties primarily manifest in the highly hydrated conditions, and once the operating temperature exceeds 80 °C, these membranes begin to deteriorate due mainly to the process of dehydration. As a matter of factor, Nafion® polymer contains the functional groups of SO_3^-, which attract cations and repel anions. These cations carry the water molecules which pass through the main chain in an electric field [19]. As the operating temperature increases close to the boiling point of water, the molecular chains of Nafion® start losing water molecules and, as a result, the membrane PC starts decreasing. Utilization of LT-PEMs in PEMFCs poses the technical challenges in terms of thermal and water management as well as maintaining the tolerance of the electrocatalysts and PEMFCs to fuel impurities, e.g., CO and SO_2, that are generated in thermal reforming of methane for H_2 [20].

To address the outstanding issues in LT-PEMFCs, elevation of the operating temperature can offer the technical merits and favorable resolutions. Firstly, higher operating temperatures can noticeably enhance the chemical reaction rates at electrodes and, thus, improve the energy conversion efficiency, potentially reduce the electrocatalyst load, and even possibly use non-platinum group (NPG) metals and alloys to replace costly Pt as catalysts. Secondly, higher operating temperatures can also improve the PC of the PEMs and, therefore, the current and power densities. Thirdly, higher operating temperatures can improve the water management in PEMFCs and avoid the notorious flooding issue commonly confronted in the cathode of LT-PEMFCs. Lastly, high operating temperatures can effectively suppress the irreversible electrocatalyst poisoning due to fuel impurities and increase the catalyst durability. Recent investigations indicate that IT-PEMFCs operated at the temperature range of 150 — 200 °C can tolerate CO gas of up to 3 % in the H_2 compared to the tolerance level of CO (10 — 100 ppm) in LT-PEMFCs [21,22].

Due to the technical limitations of Nafion® membranes at higher temperatures and low RH, non-fluorinated arylene polymers have been considered for the fabrication of IT-PEMs, because of their low cost, sound thermal stability, chemical stability, and mechanical strength. To date, a variety of polymers, e.g., polybenzimidazole (PBI), sulfonated polyether-ether-ketone (SPEEK) [23], polysulfone (PSU) [24], and polyether sulfone (PES) have been investigated for developing IT-PEMs, of which PBI is of one of the great foci by researchers [25]. PBI represents a family of thermoplastic heterocyclic aromatic polymers with excellent chemical stability, high thermal stability (T_g = 425 — 430 °C), high moisture-regaining capacity, and very good mechanical retention stability at high temperatures. Yet, PEMs developed from arylene polymers carry certain limitations. Firstly, these polymers consist of aromatic rings in their main chains, which restrict the movement of the polymer chains, resulting in reduced flexibility for ionic clustering [26]. Secondly, these membranes may exhibit low PC due to the presence of proton-conducting groups, e.g., SO_3^-, attached to the cyclic structures in the main chain. Such an arrangement may result in the challenge to achieve an optimal hydrophilic-hydrophobic balance, which is crucial to efficient proton transport [27]. One technique adopted to enhance the PC of these PEMs is to increase the degree of sulfonation (DS) [28]. Neverthless, at a higher DS, water uptake of the PEMs increases, which deteriorates the physical properties, e.g., the mechanical and dimensional stability, and, thus, limits the use of these membranes under certain operating conditions [29,30]. Thirdly, in fuel cell operation, such PEMs exhibit limited resistance to strong acids and bases because the nature of their chemical structures compromises their durability and performance of the fuel cell [31,32].

To address the challenging issues associated with IT-PEMs, several technical approaches have been investigated, including modification of the chemical structure of the polymers, polymer cross-linking, pore-filling techniques, and incorporation of nanomaterials. Among these, incorporation of nanomaterials into PEMs has gained significant attention in recent years due to its simplicity and effectiveness, as nanomaterials can reduce the gas crossover, enhance the water retention, and improve the mechanical strength and thermal stability of PEMs [33]. Inorganic materials that have been commonly used as PEM fillers include inorganic solid-state proton conductors [17], oxide NPs, carbonaceous materials, clays, and metal-organic frameworks. Metal oxide NPs, e.g., titanium dioxide (TiO_2), cerium dioxide (CeO_2) [34], silicon dioxide (SiO_2) [35], zirconium dioxide (ZrO_2), etc., have been explored for their capabilities to improve the physical stability and water retention properties of the resulting nanocomposite PEMs [36]. Table 2 lists the comparative properties of several pure PEMs and their counterparts containing metal oxide nanofillers. In addition, carbon nanomaterials, including graphene oxide, carbon nanotubes (CNTs), and carbon dots, have also been utilized to improve the physicochemical and thermal stability of PEMs [37,38]. Mesoporous materials, e.g., mesoporous silica (SBA-15) and metal-organic frameworks (MOFs), can also be used for enhancing the thermal stability and PC of IT-PEMs, which enable a well-defined pore structure that can improve the water management, facilitate the proton transport in the membrane, and hence enhance the overall performance of the fuel cells [39].

While nanomaterials have demonstrated improved functionalities in IT-PEMs, their utilization also presents certain challenges. Firstly, achieving proper dispersion of nanomaterials within the polymer matrix is a challenging process, as their aggregation can result in uneven dispersion, which hinders the expected higher PC and reduces the resulting mechanical properties [37,45]. Secondly, ensuring

Table 2
Effects of NP fillers on the properties of PEMs.

Polymer	NPs	Proton conductivity (S cm^{-1})			Tensile strength (MPa)		Power density (mW cm^{-2})		OCV (V)		Refs.
		Pure	W/NPs	Temp (°C)	Pure	W/NPs	Pure	W/NPs	Pure	W/NPs	
SPAEK	SiO_2(38 nm)	0.159	0.179	90	17.6	25.9	296.7	339.9	>0.92	>0.92	[35]
SPEEK	CeO_2(21 nm)	–	–	–	60	68.5	499	600	0.85	1.0	[40]
PA-PEI/PVA	ZrO_2((30-40 nm)	0.004	0.043	120	–	–	0.307	0.424	0.38	0.5	[36]
PBI	SiO_2 (50 nm)	0.0001	0.0039	180	48.5	67.7	–	–	–	–	[41]
PBI-OO	TiO_2 (<100 nm)	0.068	0.098	160	11 ± 4	6 ± 4	202	356	0.93	0.98	[42]
PBI	TiO_2 (1.14 μm)	0.078	0.128	125	–	–	570	800	0.83	0.83	[43]
PBI	Fe_2TiO_5 (48-70 nm)	0.048	0.078	180	80	120	280	430	0.85	0.87	[44]

*W/NPs: With nanoparticles, OCV: Open circuit voltage.
**Sulfonated poly (arylene ether ketone) (SPAEK), phosphoric acid (PA), poly (ethylene imine)/polyvinyl alcohol (PEI/PVA), and polybenzimidazole (PBI).

compatibility between the nanomaterials and polymer matrix is crucial, as lack of compatibility may lead to phase separation that adversely impacts the thermal, chemical, and mechanical properties of the resulting nanocomposite PEMs [46]. To address these issues and enhance the resulting properties of IT-PEMs, various technical approaches have been sought, including NP functionalization, size and shape screening and selection, and optimization of polymer-NP interactions. This review article primarily focuses on the main strategies for NP functionalization and its impact on the properties of IT-PEMs fuel cell applications. To the best of our knowledge, this is the first review to specifically focus on the functionalization strategies of NPs and their influences on the properties of IT-PEMs, especially the PC and hydrogen crossover.

3. Surface modifications of NPs and their roles in IT-PEMs

NPs are expected to offer the promising technical routes to improving the performance of IT-PEMs, e.g., the PC, thermal, chemical, and mechanical stability, as well as the resistance to hydrogen crossover. A number of experimental studies have demonstrated that incorporation of NPs into PEMs yields enhanced properties compared to those of the pristine PEMs [47–49]. Furthermore, NPs are capable of reducing the tortuosity inside the PEMs and therefore enhancing the proton mobility [50]. However, the high specific surface area and high surface energy of NPs can lead to their agglomeration within the polymer matrix, compromising the interfacial interactions between the NPs and the polymer matrix. Surface modification serves as an effective approach to reduce the surface energy and, therefore, improve the NP dispersion in the polymer matrix [51,52]. Surface modification involves attaching different functional groups, e.g., thiols, carboxylic acids, alcohols, or sulfonic groups, onto the NP surface by means of various physical or chemical techniques. The goal of surface modification is to enhance the interaction between the NPs and polymer chains of the polymer matrix, ultimately improving the properties of the resulting nanocomposite IT-PEMs. Several methods, including polymer and silane grafting, have been successfully employed for NP modification to enhance the properties of the resulting PEMs. The subsequent sections are to provide detailed reviews of each technique.

3.1. NP surface modification for PEMs — silane grafting technique

Silane grafting is the simplest method for functionalization of NP surfaces via grafting various functional groups. Silanes are silicone-based compounds with the general formula of R'-$(CH_2)_n$-Si-$(OR)_3$. Fig. 4 shows a single molecule of silane coupling agent containing a silicone atom, linker, organic functional group, and hydrolyzable groups. The organic functional group is responsible for the polymer matrix interaction while the hydrolyzable groups are responsible for the formation of covalent bonds with inorganic surfaces [53]. Depending upon the desired functionality, a variety of organosilanes have been used for NP functionalization, e.g., 3-aminopropyltriethoxysilane (APTES), *N*-(2-Aminoethyl)-3-aminopropyltrimethoxysilane (AEAPTS), 3-aminopropyltrimethoxysilane (APTMS), *N*-(2-aminoethyl)-3-aminopropyltrimethoxysilane (AEAPMDS), *N*-(6-aminohexyl)-3-aminopropyltrimethoxysilane (AHAPS), (3-glycidyloxypr opyl) trimethoxysilane (GPTMS) 3-mercaptopropyltrimethoxysilane (MPTMS), etc. For the purpose of use in PEMs, the preferred NPs are mostly functionalized with organosilanes bearing acidic or basic groups since these functional groups provide additional pathways for proton transport in addition to the improvement of the overall performance of fuel cells [34]. Among others, oxide NPs with –OH groups are considered as the best candidate for functionalization with a silane coupling agent as they possess high surface energy and readily form a covalent bond with a silane coupling agent.

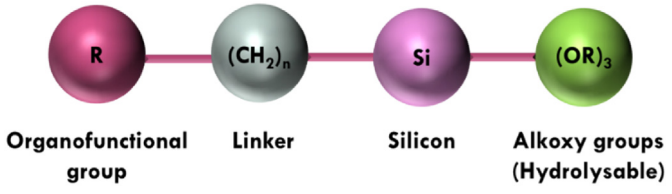

Fig. 4. The general form of a silane coupling agent.

NP surface modification involves three steps: 1) replacement of alkoxy groups with –OH groups through hydrolysis process in the acidic, basic, or neutral medium. This reaction results in the formation of silanol groups Si–OH, 2) condensation process, which involves the formation of Si–O–Si linkage with the removal of water from two or more alkoxysilane molecules, and 3) phase separation and complete attachment of silane to the substrate as illustrated in Fig. 5 [54]. The reaction rate depends typically upon the water/silane ratio, temperature, type of silane, catalyst, and pH [55].

Research efforts have been made to improve the PC of PEMs by using various modified NPs. Table 3 lists the effects of silane-modified NPs on the performance of PEMs. Salarizadeh et al. [56] fabricated SPEEK nanocomposite membranes by using amine-functionalized iron titanate (AIT) NPs. In their study, the APTES was utilized as a silane coupling agent. Results revealed that the SPEEK membrane loaded with 2.0 wt% AIT NPs showed a high PC of 0.12 S cm^{-1} at 80 °C with a power density of 204 mW cm^{-2} that was measured from a single-stack PEMFC test. The mechanical stability of such a membrane is higher than the pristine SPEEK membrane due to formation of hydrogen bonds between $–NH_2$ functional groups of AIT NPs and $–SO_3H$ groups of the SPEEK matrix [56]. Another similar study was conducted by Salarizadeh et al. [57] to optimize the operating parameters including APTES/AIT ratio, reaction time (RT), and triethylamine (TEA)/AIT ratio to obtain the maximum grafting efficiency of APTES on the surface of AIT NPs. This study indicated that the TEA/AIT and APTES/AIT ratios were the key parameters governing the grafting percentage. NP modification with a silane coupling agent can significantly reduce the NP agglomeration. Moreover, SPEEK membrane with 3.0 wt% AIT (with a maximum grafting efficiency of 6.64 %) showed an excellent PC of 0.024 S cm^{-1} at 25 °C, power density of 149 mW cm^{-2} at the cell voltage of 0.5 V and operating temperature of 80 °C, as shown in Fig. 6 [57].

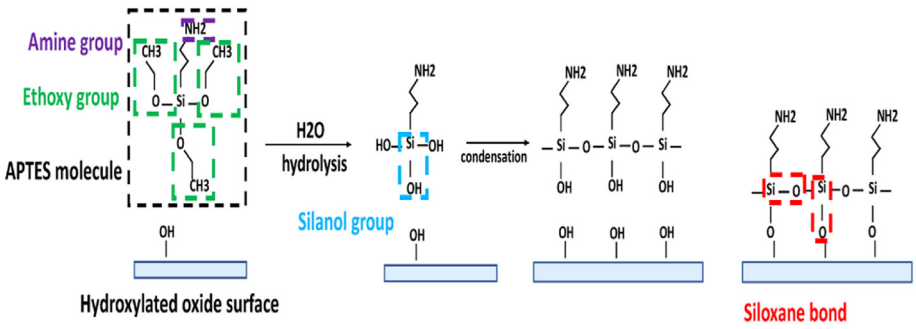

Fig. 5. Modification mechanism of an oxide surface with APTES [54].

Table 3
Effects of silane-modified NPs on the performance of PEMs.

Nanofillers	PM	CA	PC of CM (S cm^{-1})	Temp (°C)	PD of CM (mW cm^{-2})	Catalyst loading (mgcm^{-2})	Remarks	Refs
SiO_2(0.1–5μm) nanosheets	PES-PVP	MPTMS	0.0515	150	546	Pt/C: 0.75	Membrane with 0.25 wt% modified silica (S-SN) nanosheets	[58]
Fe_2TiO_5(<80nm)	SPEEK	APTES	0.12	80	204	Pt/C: 0.25	Membranes with 2.0 wt% of fillers	[56]
Co_3O_4(40–80nm)	Nafion	APTES & TEOS	0.160	90	–	-	Nafion/CO_3O_4(5 wt%) nanorods functionalized with APTES show good PC as compared to other morphologies (nanosphere, nano-octahedral)	[59]
Fe_2TiO_5(80nm)	SPEEK	APTES	0.024	25	149	Pt/C: 0.25	Membranes with 3 wt% of filler	[57]
TiO_2(<100nm)	PBI-OO	PTEOS	0.098	160	356	Pt/C: 1.00	TiO_2 modified with silane and then fuming sulfuric acid to obtain *S*–TiO_2. Membrane with 6 wt% of modified filler. PA doped membrane	[42]
$SiO_{2(-)}$	SPAEK	APTES	0.159	95	51.1	Anode (Pt/C): 3 Cathode (PtRu/C): 2	Membrane with 5 wt% of fillers	[60]
$TiO_{2(-)}$	PBI	PTEOS	0.096	150	621	–	Membrane with 2 wt% S–TiO_2. PA doped membrane PA (115 %)	[61]
$TiO_{2(-)}$	PBI	APTES	0.084	160	420	Pt/C: 0.5	Membrane with 10 wt% modified TiO_2. PA (85 wt%) loaded membrane	[62]
TiO_2(<25nm)	Nafion	MPTMS	0.067	120	–	–	Amount of fillers: 5 wt%	[63]

*Polyethersulfone (PES), polyvinylpyrrolidone (PVP), polymer matrix (PM), coupling agent (CA), composite membrane (CM), power density (PD), and open circuit voltage (OCV).

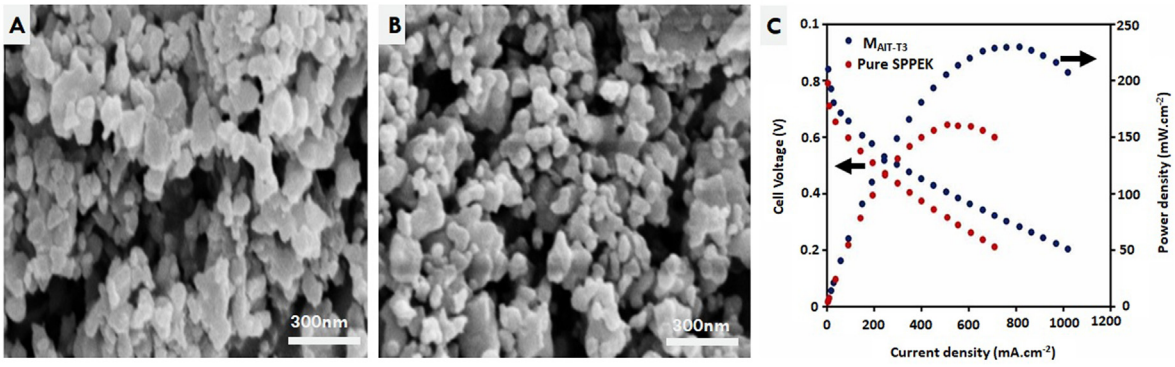

Fig. 6. A) Iron titanate NPs without APTES modification, B) Iron titanate NPs modified with APTES, and C) Single-cell performance of pristine SPEEK PEM vs 3.0 wt% AIT/SPEEK nanocomposite membrane at $T = 80$ °C and RH = 100 % [57].

Imran et al. [62] prepared the high-temperature PEMs (HT-PEMs) that were made of sulfonated PBI (sPBI) and APTES functionalized TiO_2 NPs. The optimized membrane with 10 wt% of functionalized TiO_2 NPs showed the highest PC of 0.084 S cm^{-1} as compared to bare sPBI (0.040 S cm^{-1}) under the anhydrous conditions at 160 °C. The as-prepared membrane showed superior thermal stability compared to Nafion-117 and pristine sPBI possibly because functionalized TiO_2 NPs filled up the free space between the polymer chains, increasing the membrane glass transition temperature (T_g) and improving the membrane thermal stability. Moreover, the power density of sPBI-ATI (10 wt%) was observed at 0.42 W cm^{-1} [41,62]. Pu et al. [67] developed IT-PEMs made of PBI reinforced with silane-modified SiO_2 NPs. The research showed that modified SiO_2 NPs can retain and absorb phosphoric acid (PA) which acts as the proton carrier in PBI-based PEMs. This immobilization of PA within the membrane enables more efficient transport of proton carriers. Guo et al. [58] fabricated the HT-PEMs by successfully integrating silica nanosheets (SNs) into a polyethersulfone-polyvinylpyrrolidone (PES-PVP) polymer matrix. Exfoliated silica nanosheets (*E*-SNs) were prepared by liquid-phase exfoliation method while sulfonated silica nanosheets (*S*-SNs) were obtained by surface modification of SNs using

MPTMS (Fig. 7A). Unlike silica NPs, these silica nanosheets have more –OH groups to interact with the polymer matrix and form continuous proton conducting paths. Membranes containing *E*-SN fillers have a rough surface compared to that of *S*-SNs, where interfacial compatibility is increased due to the interaction of sulfonic groups of *S*-SNs with the polymer matrix. This study revealed that at 150 °C the membranes with the optimum concentration of *S*-SNs of 0.25 wt% demonstrated the highest PC of 51.5 $mScm^{-1}$ and the power density of 546 mW cm^{-2}, compared to the membranes containing SN or *E*-SN fillers. Moreover, this study claimed that PES-PVP membranes loaded with 0.25 wt% *E*-SNs and *S*-SNs showed the open circuit voltage (OCV) of 0.91 and 0.93 V, respectively, exemplifying that these fillers enable to suppress the hydrogen crossover [58], as shown in Fig. 7 (B-D).

Lee et al. [61] developed HT-PEMs made of PBI reinforced with silane-modified sulfonated titanium dioxide (*S*–TiO_2) NPs. In their research, triethoxyphenylsilane (PTEOS) was used for NP salinization while sulfonation was made by using fuming sulfuric acid. To form the composite membranes, the as-prepared NPs were blended with PBI at varying concentrations (x = 2, 4, 6, and 8 wt%, respectively). SEM images (Fig. 8A) of the pure PBI and PBI-S-TiO_{2x} membranes doped with PA revealed that surface modification and filler concentration have a significant effect on the NP agglomeration, which directly influences the PA doping level and PC. At 150 °C, the composite PEMs demonstrated the PC of 0.096 S cm^{-1} for PBI-S-TiO_2(2 wt%) and 0.078 S cm^{-1} for pure PBI (Fig. 8B). In addition, 2.0 wt% *S*–TiO_2 loaded membrane possessed a power density of 621 mW cm^{-2}, a 30 % improvement compared to pure PBI (471 mW cm^{-2}) (Fig. 8C). It was also found that addition of NPs decreased the PA leaching, however, at higher concentrations the effect of NP fillers on the PA retention was negligible (Fig. 8D) [61].

A similar study was conducted by Krishnan et al. [42], in which *S*–TiO_2 NPs were used with PBI to develop a composite HT-PEM. It was found that thermal curing enabled to convert ionically crosslinked membranes to chemically crosslinked ones, in which *S*–TiO_2 acts as a cross-linker as well as a filler.

Furthermore, filler concentration also influences the properties of the PEMs. Li et al. [60] fabricated a series of SPAEK/NH_2–SiO_2 PEMs to evaluate the oxidative stability and fuel crossover performance at intermediate temperatures. Tetraethoxysilane (TEOS) and 3-triethoxysilylpropylamine were used to modify the surface of the mesoporous silica fillers. The performance of the membrane was enhanced due to the acid-base interaction between the organic SPAEK polymer and the inorganic mesoporous silica fillers. Oxidative stability of the membranes was improved as the concentration of modified-SiO_2 increased (from 1.0 to 7.0 wt%) since SiO_2 was more robust to hydroxyl radical attack compared to the polymer. Experimental results showed that membranes containing 5 wt% NH_2–SiO_2 NPs exhibited low methanol crossover, i.e., 11.0 × 10^{-7} cm^2 S^{-1} compared to the pristine membranes, i.e., 16.0 × 10^{-7} cm^2 S^{-1} at 80 °C [60]. The value of PC of the membrane increased up to a certain concentration level of NH_2–SiO_2 while the ion exchange capacity (IEC) reduced with increasing concentration of the fillers, as shown in Table 4.

Singha et al. [64] modified the surface of the silica NPs with a long-chain silane, i.e., *N*-(3-trimethoxysilylpropyl) diethylenetriamine (TMSPDT). The modified silica NPs (LAMS) were used to develop PBI/-LAMS nanocomposite PEMs. The PC of the PA-doped pure PBI membranes was measured 0.118 S cm^{-1} while for PBI/LAMS (15 wt%) acid-doped composite membranes the PC was measured as 0.181 S cm^{-1} (with the increase higher than 1.15 folds). The long-chain silane with three amine groups improves the PC due to the formation of hydrogen bonds with PBI chains and crystallites throughout the matrix, which provided continuous channels for the proton transport [64].

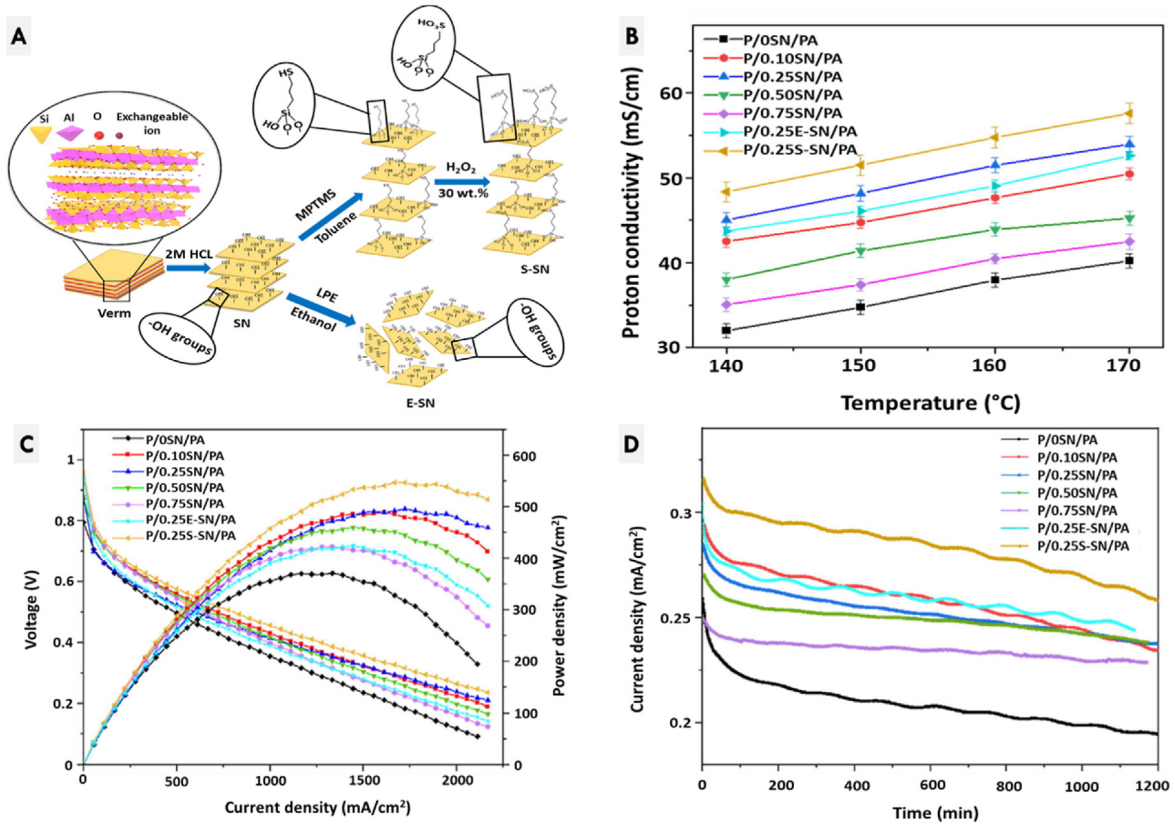

Fig. 7. A) Synthesis of silica nanosheets (SNs) by liquid–phase exfoliation method and silane condensation, B) PCs of SNs loaded with PES-PVP, C) Polarization and power density curves, and D) Durability test at 0.60 V at 150 °C for 1200 min [58].

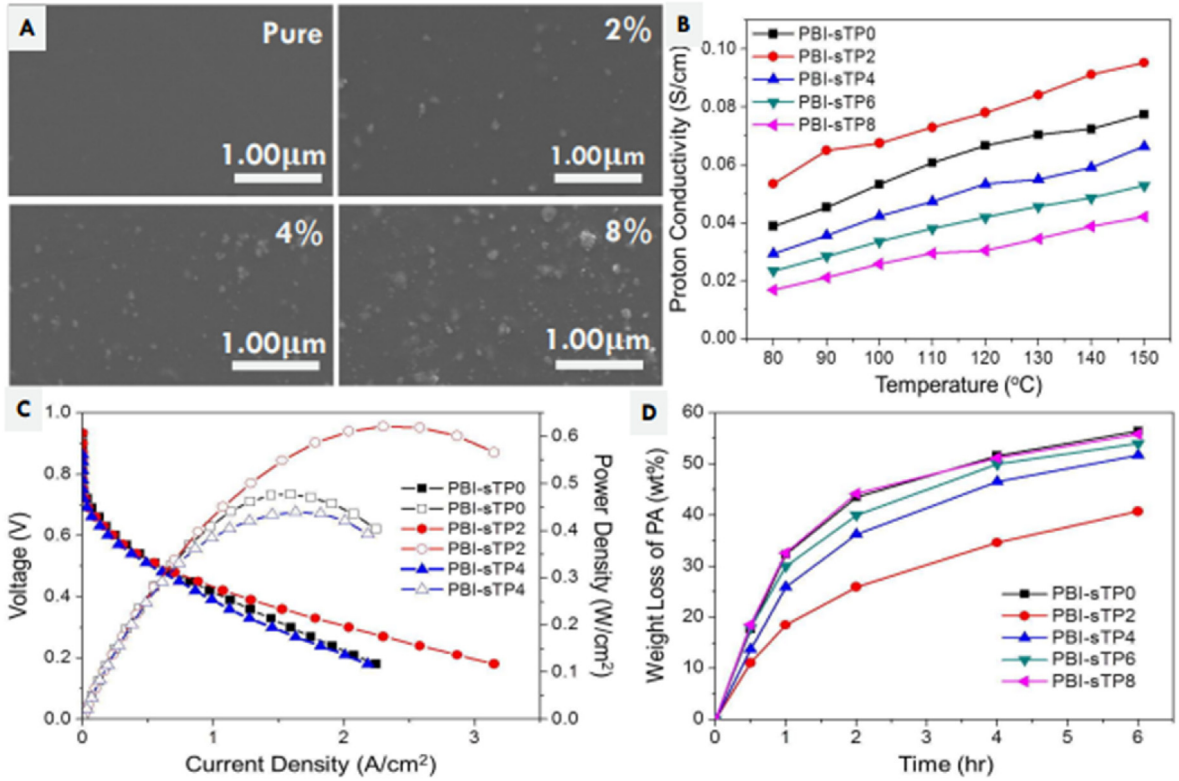

Fig. 8. A) SEM micrographs of pure PBI and PBI-S-TiO_{2x} membranes doped with PA of varying mass fractions, B) PC of the nanocomposite membranes at 150 °C, C) Polarization and power density curves, and D) PA retention of the nanocomposite membranes [60].

Table 4
Effect of the filler concentration on the properties of PEMs [60].

PEMs	IEC (mequiv g^{-1})	Proton conductivity (mS cm^{-1}) @ 95 °C	Oxidative stability (%)
SPAEK	1.18 ± 0.01	0.04	95.5
SPAEK/ NH_2–SiO_2(1 wt %)	1.17 ± 0.02	0.10	96.6
SPAEK/ NH_2–SiO_2(3 wt %)	1.00 ± 0.02	1.11	97.5
SPAEK/ NH_2–SiO_2(5 wt %)	0.87 ± 0.02	1.59	97.8
SPAEK/ NH_2–SiO_2(7 wt %)	0.68 ± 0.02	1.33	98.1

3.2. NP surface modification for PEMs—Polymer grafting technique

In this polymer grafting technique, the NP surface is modified with the polymer chains to avoid NP agglomeration and enhance the PC of the resulting PEMs. Grafting polymer chains to/from the NP surface results in a variety of hybrid nanoarchitectures, e.g., core-brushes and core-shells, among others. In core-brush nanoarchitecture, individual polymer chains with a controlled chain length are attached onto the NP surface. These polymer chains are free to move. In the case of core-shell nanostructures, the NP surface is covered with a compact polymer shell. Polymer grafting involves two main approaches: grafting-to and grafting-from. In the "grafting-to" approach, the polymer chains and the NPs are synthesized individually and then combined [65]. Usually, the functionalized end of the polymer reacts with the reactive sites of the NPs and forms a covalent bond. "Grafting-from" approach involves the in-situ growth of the polymer chains from the initiators that are previously attached onto the NP surface [66]. Both modification approaches are illustrated in Figs. 9 and 10, respectively.

Although "grafting-to" approach is more versatile and easier to implement such that it enables to attach a variety of polymers without any specific polymerization, the main disadvantage is that high molecular weight chains cannot be grafted at the high grafting densities due to the steric hindrance of polymer chains. On the contrary, "grafting-from" approach allows the higher grafting densities owing to the direct growth of the polymer chains from NP surface, making it most commonly used for NP surface modification [67]. Controlled radical polymerization (CRP) plays an important role in controlling the grafting sites, grafting densities, and thickness of the polymer brushes at NP surface. So far, four different CRP techniques have been commonly used for NP modification, i.e., reversible addition-fragmentation chain transfer polymerization (RAFT), atom transfer radical polymerization (ATRP), reversible chain transfer polymerization (RCTP), and nitroxide-mediated radical polymerization (NMRP) [67]. Among others, RAFT and ATRP are considered as the two most powerful controlled polymerization techniques. Tables 5 and 6 summarize a few literature studies that employed these polymerizations to modify NP surface with polymers containing proton-conducting groups for the purpose of use in IT-PEMFCs.

3.2.1. NP surface modification by ATRP and RAFT polymerizations

Park et al. [68] fabricated the bifunctional NPs (TiO_2-PSSA) by grafting poly (styrene sulfonic acid) (PSSA) on the surface of TiO_2 NPs utilizing ATRP polymerization. Four different concentrations (2, 4, 6, and 8 wt%, respectively) of modified NPs were mixed with P(VDF-co-CTFE)-g-PSSA copolymer to develop the nanocomposite IT-PEMs. Experimental results show that increasing the concentration of TiO_2-PSSA NPs enhances the water uptake and PC of the membranes (~4.0–5.0 × 10^{-2} S cm^{-1}) (Fig. 11A and B). At an elevated temperature, the PC of the resulting P(VDF-co-CTFE)-g-PSSA/TiO_2-PSSA(8 wt%) membranes is more prominent compared to the pristine membranes due to the caging effect and formation of hydrogen bonds, which enables the membranes capable of

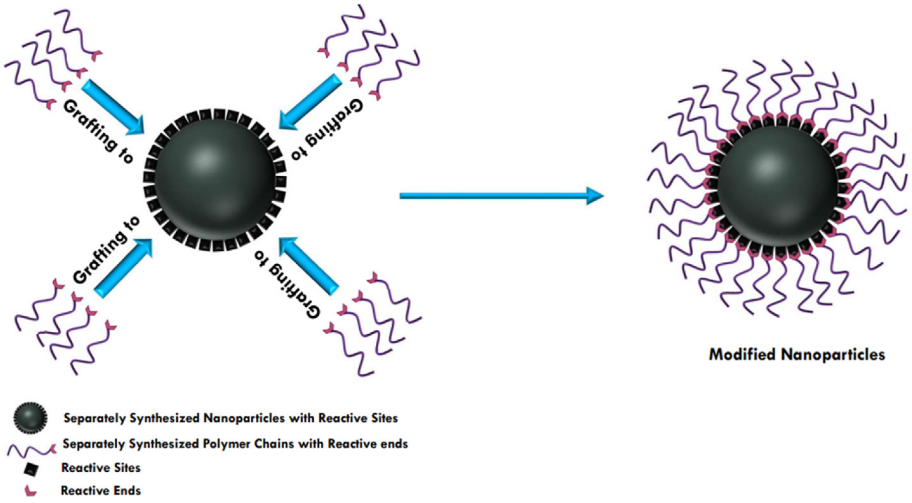

Fig. 9. "Grafting-to" approach for surface modification of NPs.

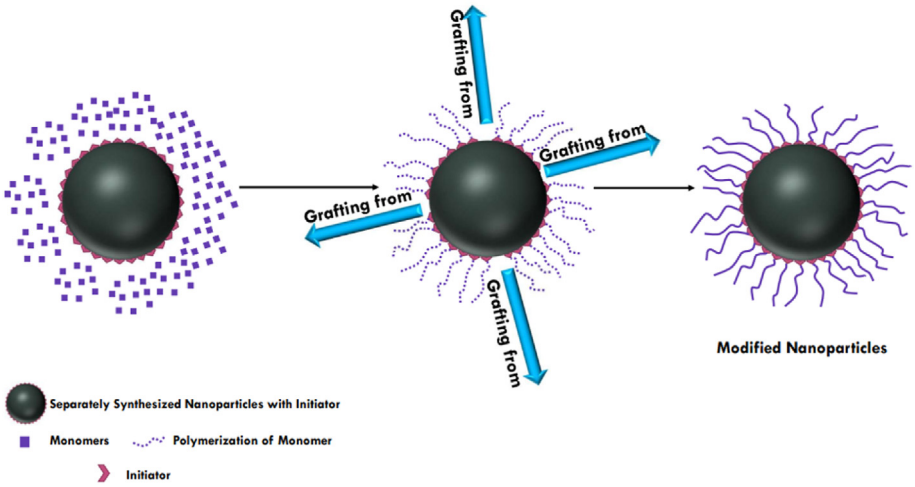

Fig. 10. "Grafting-from" approach for surface modification of NPs.

Table 5
Nanofiller modification by means of the ATRP technique.

Nanoparticles	Graft polymer	Catalyst	Matrix polymer	Initiator	Refs
TiO_2(–)	PSSA	CuCl	P(VDF-co-CTFE)-g-PSSA	CPC	[68]
SiO_2(260nm)	Poly (MeOEGMA)	CuCl, $CuBr_2$	Nafion	BIBr	[69]
SiO_2(7nm)	PVBP	CuCl	PVDF-HFP	CPMS	[70]
SiO_2(260nm)	P (MAA-co-DVB-co-CMSt)- g-PSt-SO_3H	CuCl	SPEEK	MPS	[71]
SiO_2(7nm)	PSS	CuCl	SPAES	CPMS	[72]
SiO_2(5–15nm)	PSSA, PAMPS	CuBr	PVA	APTES	[73]
SiO_2(358.2nm)	PSSA and PSPM	$CuCl_2$, CuCl, CuBr	–	APTES	[74]

withholding the water molecules strongly at higher temperatures, as shown in Fig. 11C [68].

Farrukh et al. [69] presented polymer-brushed functionalized silica NPs (SiO_2-polymer brushes) as a humidifying nano-additive for Nafion® PEMs. At a temperature of 25 °C and 20 % RH, nanocomposite membranes containing 1.0 wt% of SiO_2-polymer brushed NPs indicated the value of PC with 11 times higher than that of a control sample of the pristine Nafion® membranes. At a moderate temperature of 55 °C and 80 % RH, the PC of the nanocomposite membranes was three times higher than that of a control sample of the pristine Nafion® membranes, as shown in Fig. 12(A-B). Furthermore, the methanol crossover in the nanocomposite membranes (2.09×10^{-6} cm^2 S^{-1}) was comparable to that of the Nafion-117 membranes (2.09×10^{-6} cm^2 S^{-1}), as shown in Fig. 12C-D [69].

Labalme et al. [70] synthesized phosphonic polymer-modified silica NPs by ATRP polymerization. Several concentrations (from 10 to 60 wt %) of the modified silica NPs were used as the fillers in PVDF-HFP-based PEMs. This experimental study revealed that the membranes with 40 wt % silica loading exhibited the highest PC value of 65 mS cm^{-1} at 80 °C, due to the low IEC (1.08 meq g^{-1}) of the membranes [70].

Zhang et al. [71] used hollow microspheres modified with sulfonated polystyrene (PS) through SI-ATRP polymerization. The synthesis process consists of a few steps as follows: silica NPs were first modified with 3-(methacryloxy) propyltrimethoxysilane (MPS) to obtain MSP-SiO_2 NPs. The as-prepared MSP-SiO_2 NPs were used as seeds to graft the copolymer poly (methacrylic acid-*co*-divinylbenzene-*co*-4-chloromethyl styrene) to obtain the core-shell microspheres SiO_2@P (MAA--co-DVB-co-CMSt). Then, ATRP polymerization was used to graft PS from the surface of SiO_2@P (MAA-co-DVB-co-CMSt) leading to the formation of SiO_2@P (MAA-co-DVB-co-CMSt)-g-PSt microspheres. Sulfonation of

Table 6
Nanofiller modification by means of the RAFT technique.

Nanoparticles	Graft polymer	RAFT agent	Matrix polymer	Initiator	Refs
SiO_2(60nm)	VImBr	CPDB	OPBI	AIBN	[75]
SiO_2(235nm)	PVPA-b-PS	O-ethyl-*S*-(1-ethoxycarbonyl)-ethyldithiocarbonate	Polycarbonate	AIBN	[76]
SiO_2(100nm)	PAA-b-PS	CMDT	-	MeO-AMVN, AIBN	[77]
SiO_2(100,300,500nm)	PAA-b-PS	CMDT	-	AIBN	[78]
SiO_2(47±2nm)	PNVT-g-PNVI and PNVI-g-PNVT	CPDB	OPBI	ACP	[79]
SiO_2(50,100nm)	PNVI	CPDB	OPBI	AIBN	[80]
SiO_2(200nm)	PAA-g-PS	CMDT	–	2,2′-azobis (4-methoxy-2,4-dimethylvaleronitrile)	[81]
SiO_2(200nm)	PAA-b-PS	CMDT	–	AIBN	[82]

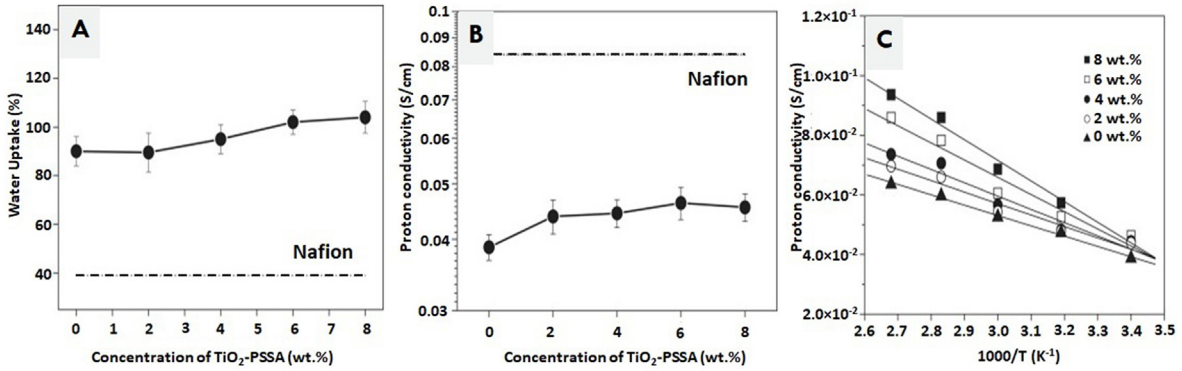

Fig. 11. A) Water uptake of the membranes as a function of the concentration of modified NPs, B) PC of the membranes as a function of NP concentration at room temperature, and C) Arrhenius plot for the PC of the membranes at higher temperatures [68].

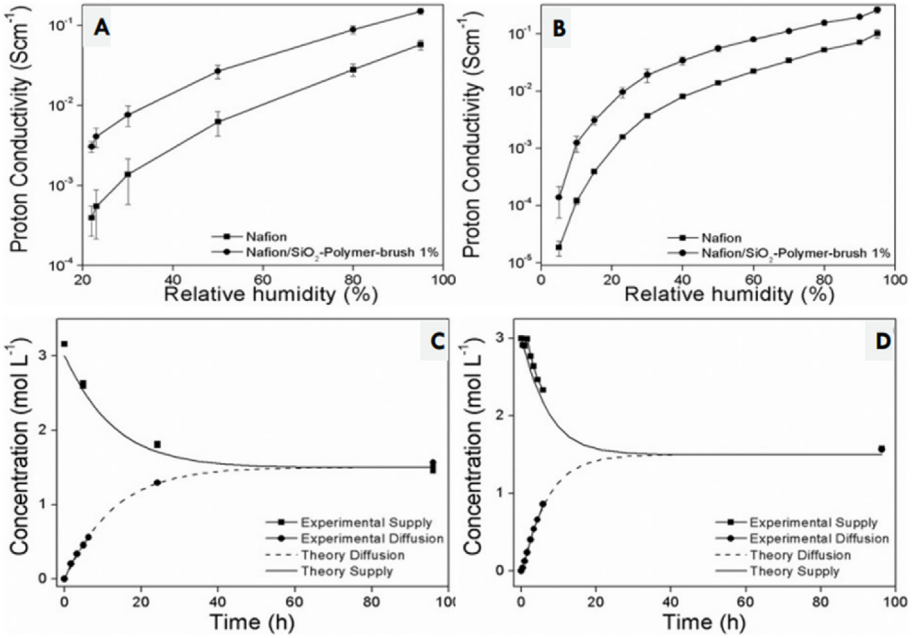

Fig. 12. A) Effect of humidity on the PC of the pristine Nafion® membranes and Nafion®/SiO_2-polymer-brush 1.0 wt% at 25 °C, B) Effect of humidity on the PC of the pristine Nafion® membranes and Nafion®/SiO_2-polymer-brush 1.0 wt% at 55 °C, C) Methanol permeability of Nafion-117, and D) Methanol permeability of Nafion/SiO_2-polymer-brush 1.0 wt% [69].

these microspheres was done by sulfuric acid (H_2SO_4) with further removal of the core (SiO_2) by etching the microspheres with hydrofluoric acid (HF) to obtain hollow P (MAA-co-DVB-co-CMSt)-g-PSt-SO_3H microspheres (HPSS). HPSS was mixed with SPEEK polymer to fabricate the hybrid PEMs. These hybrid membranes possess 83.3 % PC of 33 mS cm^{-1} compared to the pure SPEEK membranes (18 mS cm^{-1}) at 75 °C and 100 % RH. Due to the strong interactions between the HPSS and SPEEK matrix, the composite membranes loaded with 15 wt% HPSS showed a 42.5 % reduction in methanol permeability compared to the pristine SPEEK membranes, as shown in Fig. 13 [71]. Park et al. [72] grafted

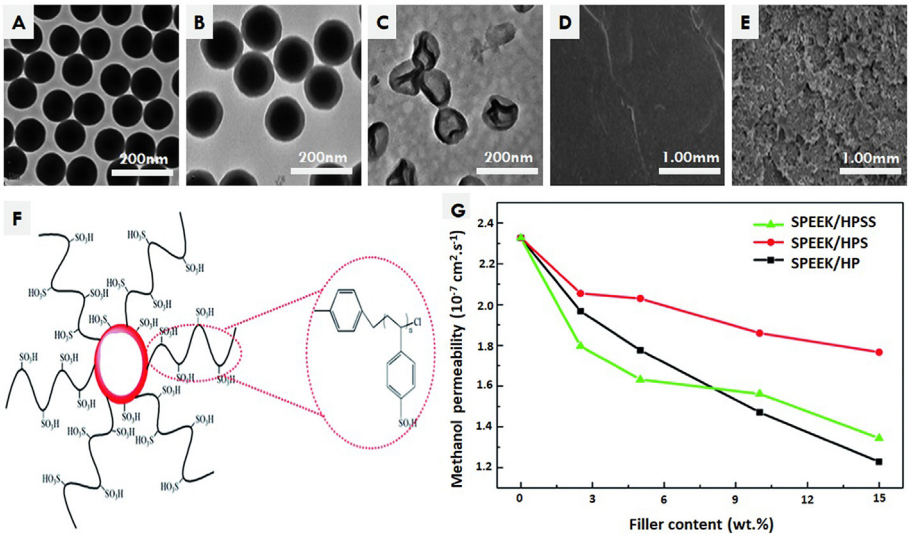

Fig. 13. A) TEM micrograph of MPS-SiO_2 microspheres, B) TEM micrograph of core-shell microspheres SiO_2@P (MAA-*co*-DVB-*co*-CMSt)-*g*-PSt, C) TEM micrograph of HPSS, D) SEM micrograph of the SPEEK membrane sample, E) SEM micrograph of the hybrid membrane with 15 wt% HPSS, F) Chemical structure of the HPSS microsphere, and G) Methanol permeability of the hybrid membranes [71].

polystyrene sulfonate (PSS) on the surface of silica NPs (PSS-*g*-SiO_2). The nanocomposite PEMs (CPS/PSS-g-SiO_2) were fabricated by blending several concentrations of modified NPs with sulfonated poly (arylene ether sulfone) (SPAES) copolymer. By comparison with the commercially available Nafion-112, a nanocomposite membrane reinforced with 10 wt % of PSS-g-SiO_2 NPs demonstrated a superior current density of 690 mA cm^{-2} at the voltage load of 0.6 V, operating temperature of 120 °C, and RH of 30 % [72].

Koyilapu et al. [75] modified the surface of SiO_2 NPs with poly (vinylimidazolium) bromide (PVImBr) brushes by means of the RAFT polymerization technique to determine the effect of the grafting polymer chain length and the grafting amount on the properties of poly (4, 4′-diphenylether-5,5′-bibenzimidazole) (OPBI) membranes. Two types of modified silica NPs were prepared by altering the concentration of VImBr monomer during the reaction process. Silica NPs with the lower molecular weight and the lower amount of polymer grafting were abbreviated as PVImBr(L)-g-SiNP while the NPs with the higher molecular weight and the higher amount of polymer grafting were abbreviated as PVImBr(h)-g-SiNP. A strong interfacial interaction between the PVImBr grafted SiNP and polymer matrix was observed. Moreover, NP aggregates were evenly distributed throughout the membrane, creating a dense network in the polymer matrix. Experimental results showed that the PC increased with increasing NP concentration up to 0.25 mS cm^{-1} for the membrane fabricated with 10 wt% of PVImBr(H)-g-SiNP and 0.21 mS cm^{-1} for the membrane fabricated with the 10 wt% of PVImBr(L)-g-SiNP at 160 °C. The higher grafting amount of the PVImBr chains facilitated more cationic head groups available to interact and hold the PA molecules in the membranes, which results in less acid leaching at higher temperatures, e.g., 30 % weight loss in the membranes with 10 wt% of PVImBr(H)-g-SiNP, as shown in Fig. 14 [75].

Tobata et al. [76] constructed the 2D channels by grafting poly (vinylphosphonic acid)-*block*-polystyrene (PVPA-*b*-PS) on the NP surface and then used these NPs to construct the 3D channels via filling them with polycarbonate to form a nanocomposite membrane. It was demonstrated that the thickness of the grafted polymer membrane had a significant effect on the PC and the activation energy of the modified NPs. The PC values of the surface-functionalized NPs and nanocomposite membranes were measured as 1.3×10^{-2} and 1.8×10^{-4} S cm^{-1}, respectively, at the testing temperature of 80 °C and RH of 95 %. Moreover, the hydrophobic nature of the grafted polymer and the matrix plays a critical role in the stability of PC of both modified NPs and the nanocomposite PEMs as shown in Fig. 15 [76].

RAFT polymerization with particles (PwP) was used by Koseki et al. [77] to prepare the core-shell proton-conducting material for polymer-based PEMs. Block copolymer (polyacrylic acid-*b*-polystyrene, PAA-*b*-PS) was used to modify the surface of SiO_2 NPs. The study showed that silanol groups acted as anchoring points and proton-conducting pathways at the interface of PAA-SiO_2 NPs (Fig. 16A). Moreover, the density of these silanol groups has a significant effect on the proton-conducting performance. Surface silanol density increases by processing SiO_2 NPs with NaOH and decreases by heating at high temperatures. The PC of I-silica@PAA-PS (4.62×10^{-3} S cm^{-1} @ 98 % RH and 60 °C) was higher compared to other NPs due to the high density of silanol groups (Fig. 16B). Furthermore, the inter-silanol distance in the case of *P*-silica@PAA-PS and I-silica@PAA-PS is closer to the ideal inter-silanol distance, i.e., 7.23 Å, thus chance was increased to form hydrogen bonds between the silanol groups of SiO_2 NPs and the carboxylic groups of polyacrylic acid. Such proton hopping mechanism enhanced the PC value (Fig. 16C) [77].

Nohara et al. [78] reported that the PC of PEMs with polymer-modified nanofillers was highly dependent on the core size of the nanofillers. In their research, silica NPs with three different sizes of 100, 300, and 500 nm, respectively, were functionalized using PAA-b-PSS polymer. It was found that decreasing NP size increased the proton-conducting pathways, which contributed to the PC enhancement and the reduction of the activation energy. Silica(100)@PAA-b-PS showed a higher PC value of 1.04×10^{-3} S cm^{-1} and a low activation energy of 0.227 eV while Silica(500)@PAA-b-PS showed the lowest PC value of 2.57×10^{-4} S cm^{-1} and the highest activation energy of 0.307 eV, as shown in Fig. 17 [78].

Kutcherlapati et al. [80] synthesized poly (*N*-vinyl imidazole) grafted silica NPs (PNVI-g-SiNPs) by means of RAFT polymerization to fabricate PNVI-*g*-SiNPs/PBI nanocomposite PEMs. Two different concentrations (1.0 and 3.0 wt%, respectively) of NPs with a diameter of 50 — 100 nm were used to prepare PA-(85 wt%) doped nanocomposite membranes. These membranes possessed superior properties compared to those of the pristine PBI membranes. 3.0 wt% PNVI-g-SiNPs/PBI membranes showed a higher PC value of 0.14 S cm^{-1} at 180 °C due to the anisotropic self-assembled structure of nanofillers that provided continuous proton-conducting paths (Fig. 18). Owing to the more basic behavior of the PNVI chains, acid leaching of the nanocomposite membranes was less compared to the pristine membranes. As a result, the 3.0 wt% PNVI-g-SiNPs/PBI membranes carried the highest tensile strength compared to the pristine membranes as shown in Fig. 18 (B–C) [80].

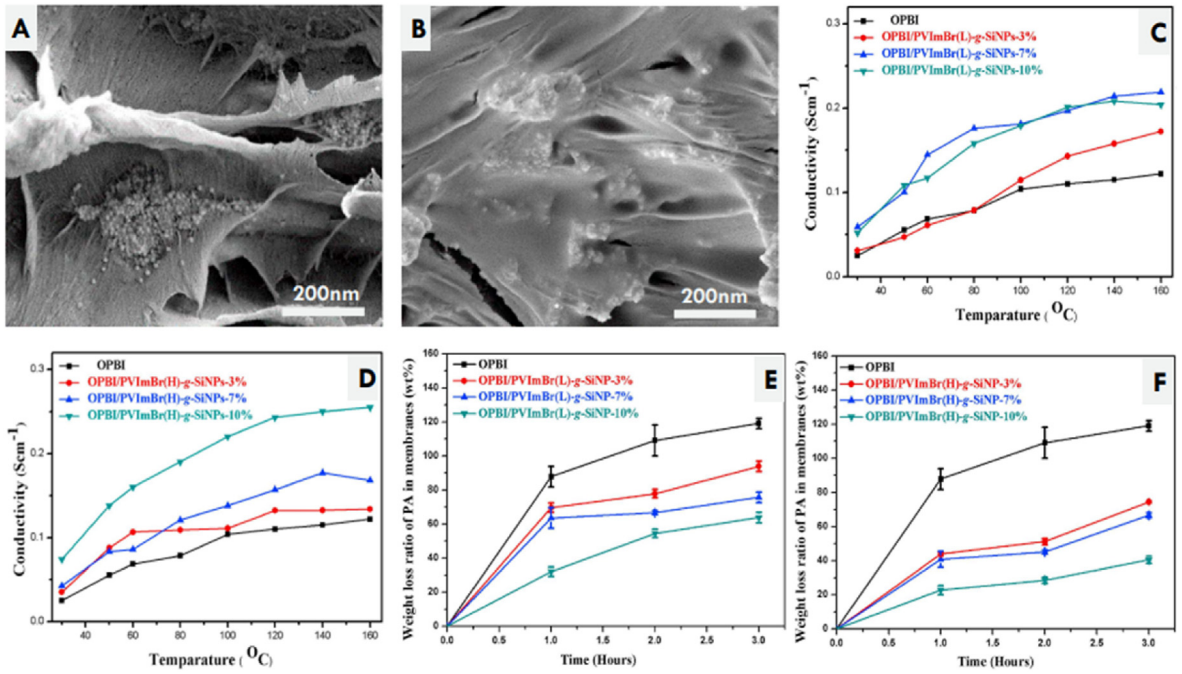

Fig. 14. A and B) SEM micrographs of the cross-sectional membranes loaded with 10 wt% of PVImBr(L)-g-SiNP and PVImBr(h)-g-SiNP, respectively, C) and D) Proton conducting properties of the membranes containing PVImBr(L)-g-SiNP and PVImBr(h)-g-SiNP, and E) and F) PA leaching behavior of the membranes containing PVImBr(L)-g-SiNP and PVImBr(h)-g-SiNP [75].

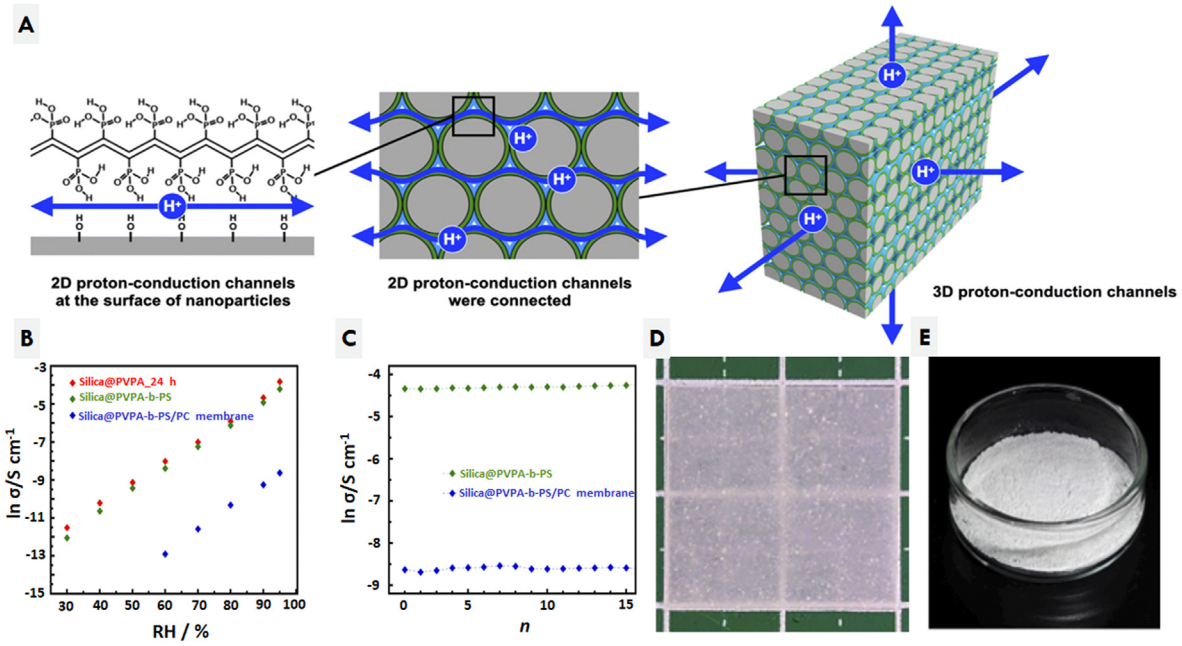

Fig. 15. A) Schematic diagram of the core-shell NP filled PEM, B) Variations of the PC value with respect to the humidity, C) PC stability of the silica NPs and PEM, D) Optical image of a PEM sample, and E) Optical image of modified NPs [76].

4. Challenges and future prospects

In the above, a detailed review has been made on several types of functionalized NPs for use as the reinforcing phase to improve the proton-conducting performance of LT- (room temperature to 120 °C) and IT-PEMs (120 — 160 °C) and related durability. Technologically, it is more compelling to enhance the PC, electrochemical durability, and structural integrity of IT-PEMs with the operating temperatures >160 °C or even 300 °C due to their merits in excellent water and heat management, high reaction rate, high power density, and superior immunity to electrocatalyst poisoning. To date, IT-PEMs are based mainly on H_3PO_4-doped PBI and other HT engineering polymers as well as IT polymer-inorganic composite (PIC) PEMs made of solid-state proton conductor powder blended with a small amount of HT polymers as the polymeric binder, e.g., PBI [17,83–86]. For H_3PO_4-doped PBI membranes that have been operated in the IT range of 120 — 180 °C (e.g., the membrane coined with Celtc® by BASF Fuel Cell, Germany), long-term cell tests of 13,000 — 18,000 h showed that the degradation is due

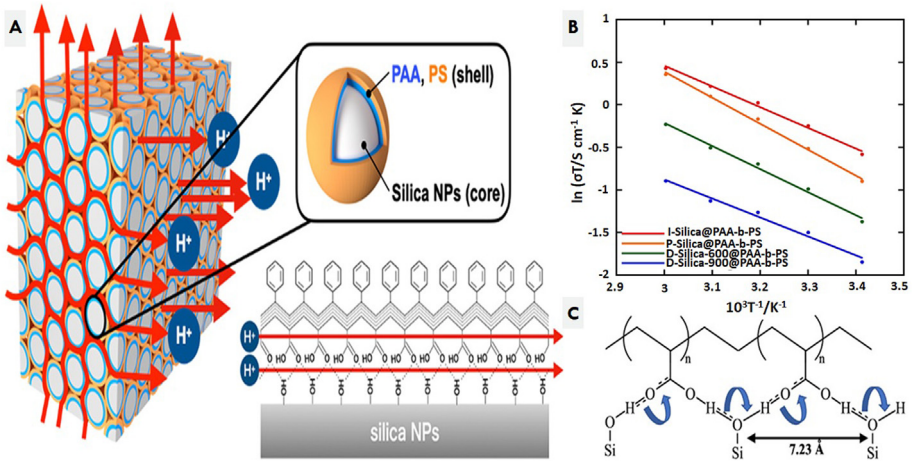

Fig. 16. A) Function of silanol groups in silica@PAA-b-PS NPs, B) Effect of silanol densities on the PC of silica NPs, C) Ideal inter-silanol group distance and proton hopping mechanism [77].

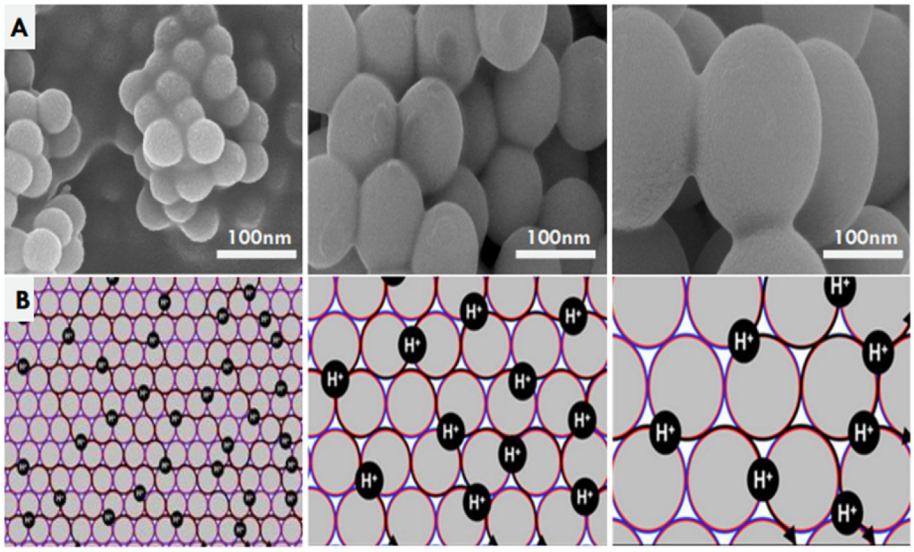

Fig. 17. A) SEM micrographs to show the core size effect on the compactness of silica-PAA-b-PS NPs with the diameters of 100, 300, and 500 nm, respectively (left to right), and B) Schematic proton transport at varying NP size increasing from the left to right [78].

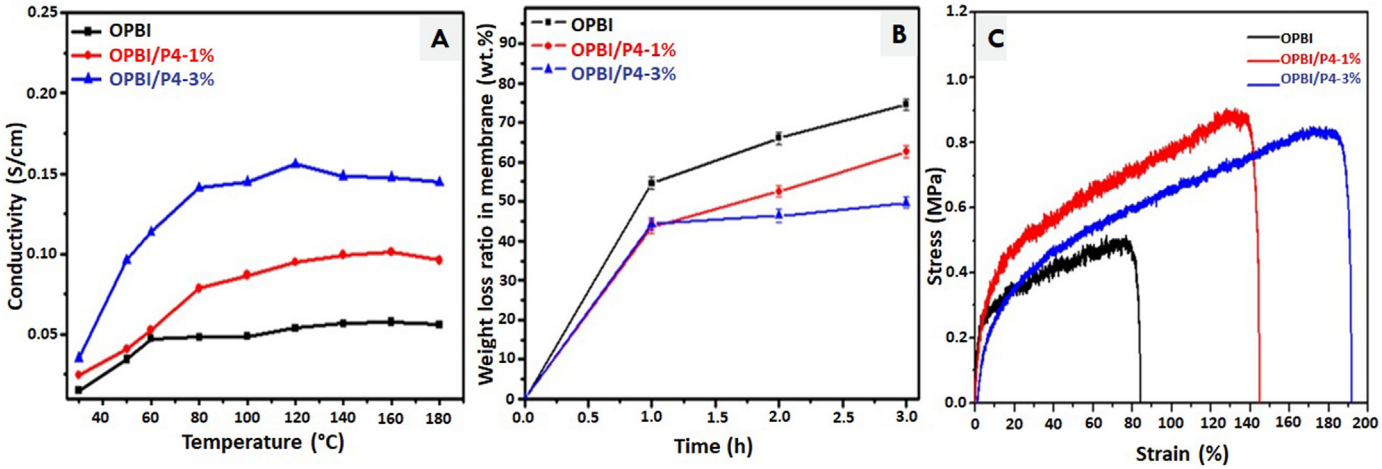

Fig. 18. A) The PC values of the pristine and nanocomposite PEMs at varying temperatures, B) Acid leaching behavior of PEMs, and C) Tensile mechanical properties of the pristine and nanocomposite PEMs [80].

mainly to acid loss, membrane thinning caused by polymer degradation, etc. [87,88]. For these acid-doped PBI membranes, incorporation of inorganic NP fillers of silica (SiO_2), zirconia (ZrO_2), titania (TiO_2), etc. can retain water and H_3PO_4 in the membranes at the higher operating temperatures due to the high adsorption capability of the inorganic nanoscale phase [43,87–93]. In addition, experimental studies also showed that addition of regenerative free radical scavengers, e.g., 2 wt% ceria NPs (CeO_2), into the PBI membranes can double the chemical stability of PBI and therefore enhance the performance durability of the PBI-based IT-PEMFCs [94]. Additional research is still needed to explore various low-cost NPs with proper surface modifications to work as nanofillers in these IT-PEMs for performance enhancement, including formulation of low-cost, effective, and rational routes to synthesis, surface modification, processing, characterization, and final deployment of nanostructured PIC membrane systems.

In addition, a variety of solid-state proton-conductors are under intensive investigation for developing high-performance IT-PIC-PEMs. Among these, heteropolyacids, e.g., $H_3PW_{12}O_{40}$, $H_4SiW_{12}O_{40}$, $H_4GeW_{12}O_{40}$, $H_6CoW_{12}O_{40}$, $H_5BW_{12}O_{40}$, etc., can be blended with PBI to form IT-PIC-PEMs to operate at 150–200 °C [83,95–99]. To further elevate the operating temperature in the IT range from 150 to 400 °C, pyrophosphates and diphosphate of tetravalent elements (MP_2O_7 with M = Sn, Zr, Ti, and Ce, respectively) doped with a small quantity of low valency cations, e.g., In^{3+}, Al^{3+}, Mg^{2+}, Sb^{3+}, Sc^{3+}, and Ga^{3+}, showed the PC value of $>10^{-2}$ S cm^{-1} [100–106]. Furthermore, recent studies have also indicated that metal ultraphosphate (e.g., CeP_5O_{14}) carried even higher PC in a wider IT range [17,86,107]. Yet, these solid-state proton conductors are fragile powders that are synthesized via thermal chemical reaction at temperatures of >600 °C and they cannot directly form durable membranes for use as PEM in PEMFCs. Thus, it is a rational option to form flexible PIC membranes to synergically exploit the high value of PC of the inorganic solid-state proton conductors and the high mechanical flexibility and durability of the HT polymers, e.g., PBI. Since PBI is a HT hydrophilic thermoplastic polymer, it can function as an excellent HT polymeric binder. Such PIC membranes can be fabricated by using low-cost solution-casting technique [19,86,108]. Yet, these IT PIC PEMs also pose new technical challenges that could be resolved by using nanotechnology, especially by using functionalized NPs.

To achieve the high-performance IT-PIC-PEMs, the mass fraction of the solid-state proton conductors should be high, e.g., as high as 75 wt% as used in Ref. [17], and the particle size of the solid-state proton conductor powder should be as small as possible for the low membrane thickness, high gas impermeability, and the high mechanical stability and structural integrity. Thus, besides reduction of the particle size of the solid-state proton conductor powder, new nanosized fillers with surface modification can be synthesized to enhance the water retention, to fill and bridge the micro and nanocavities between the particles and polymer matrix, to improve the membrane gas impermeability, and to scavenge the radicals attacking the polymer chains. It can be expected that incorporation of novel NPs with specific surface modifications into IT-PIC-PEMs would resolve the outstanding technical issues of the high-performance IT-PIC-PEMs under development for use in high-efficiency electrochemical energy conversion devices.

Moreover, as reviewed in the above, experimental investigations of the roles of functionalized NPs in performance improvement of PEMs and PEMFCs provide rich performance data and reinforcing mechanisms that can be used for developing multi-physics models to simulate, predict, and optimize the performance of NP-reinforced PEMs, since PEM is a functional material that works in the severe environment with combined mechanical, thermal, electrical, and oxidative factors. So far, no universal models are available in the literature that are capable of uniformly examining all these combined factors. However, research progresses in neighboring fields, e.g., structural polymer nanocomposites, could be employed for exploring the rational understanding of one or two performance characteristics, e.g., elastic modulus, proton conductivity, etc., of LT- and IT-PEMs made of NP-reinforced polymers. For instance, coarse-grained atomic and molecular dynamics modeling has been broadly used for predicting the tensile modulus and strength, viscosity, T_g, and failure process of NP-reinforced polymers with varying extent of consideration of the NP mass fraction, size effect, surface modification, NP-polymer interactions, etc. [109–113], which can be equivalently used for predicting the mechanical behavior of NP-reinforced PEMs. In addition, thermodynamics and molecular dynamics modeling have also been used for simulation of the transport of water and hydronium ion (H_3O^+) and hydrogen in NP-reinforced polymeric PEMs and understanding of the proton-conducting mechanisms and dependencies of proton conductivity upon various parameters, e.g., types, size, and surface modification of NPs at the atomic and molecular levels [114–118]. In addition, simple mixing rules of composite materials have also been used for simple estimates of the upper and lower bounds of the effective proton conductivity, gas crossover resistance, modulus, specific heat, heat diffusivity, etc. [119–126]. These models built upon varying scales can be used to rationally predict the single-field performance of NP-reinforced PEMs under idealized conditions. Additional modeling efforts are still desired to incorporate the nonlinear effects of NPs and their surface-functionalized counterparts into multi-field models to address the mechanical, electrochemical, and thermal response of the NP-reinforced PEMs subjected to instantaneous external current loads, especially taking into account the membrane defects, microdamage, and degradation mechanisms. In the particular case of IT-PIC-PEMs, the mass fraction of the solid-state proton conductors is as high as 75 wt% [17], and the classic micromechanics models based on assumption of weak particle interaction are not workable and thus formulation of new pure computational multi-field models would be necessary for performance prediction.

5. Concluding remarks

It is technologically important to develop PEMs with high PC, excellent thermal, electrochemical, and mechanical stability, and low hydrogen crossover for low-cost, broad applications in LT and IT electrochemical energy conversion devices, e.g., fuel cells, electrolyzers, electrochemical sensors, and electrochemical membrane reactors (e.g., low-pressure electrolytic ammonia synthesis, electrochemical CO_2 capturing, etc.), among others. In particular, to develop new generation IT-PEMs with the operating temperatures ranging from 200 to 350 °C can bridge the temperature between the commonly used LT/IT-PEMs (e.g., Nafion®-based PEMs of <100 °C and H_3PO_4-doped PBI of <160 °C) and solid oxide ionic films (>600 °C). IT-PEMFCs installed with high-performance IT-PEMs can carry the technical merits of both LT-PEMFCs (e.g., high PC, fast response, high durability, and low material constraints for electrodes and bipolar plates) and HT-PEMFCs (e.g., low catalyst load, potential use of NPG metals as electrocatalysts, high energy conversion efficiency, and excellent water and heat management). To date, there are still several outstanding technical issues of LT-, IT-, and HT-PEMFCs that need to be resolved in low costs for the purpose of low-cost, fast, and broad development and deployment of high-performance fuel cells as either stationary or mobile electrical power sources in various applications, including high-efficiency electricity generators in decentralized power stations, fuel cell ground vehicles, unmanned aerial and undersea vehicles, marine ships, mobile electrical power stations to support military missions, etc.

This review has provided one of the important technical routes to improving the performance of polymer-based LT- and IT-PEMs by incorporating surface-modified NPs, including enhancement of the PC and thermal stability, reduction of gas crossover, suppression of chemical degradation due to radical attacks, and improvement of PEM performance durability. Two low-cost practicable techniques for surface functionalization of a variety of NPs, i.e., silane grafting and polymer grafting (termed as the ATRP and RAFT polymerization techniques), have been reviewed in detail, effects of the surface-functionalized NPs on the performance improvements of LT- and IT-PEMs are compared, and related

reinforcing mechanisms are discussed and justified. The comparative study of the research data available in the literature indicates that incorporation of surface-functionalized NPs is a promising, low-cost technique that can be refined and depolyed for enhancing the performance of LT-PEMs and LT-PEMFCs. Nevertheless, very limited experimental data are available in the literature for performance improvement of polymer-based IT-PEMs that were reinforced with surface-functionalized NPs. Thus, research efforts are still desired to explore novel, low-cost techniques, including incorporation of surface-modified NPs into IT-PEMs and IT-GDLs, to improve the performance of IT-PEMs, IT-PEMFCs, IT-electrolyzers, etc., especially PC enhancement, reduction of gas crossover, and related performance retention in long-term operation.

CRediT authorship contribution statement

Abdul Salam: Data curation, Formal analysis, Validation, Visualization, Writing – original draft, Investigation, Methodology. **Oksana Zholobko:** Investigation, Methodology, Validation, Writing – review & editing. **Xiang-Fa Wu:** Conceptualization, Data curation, Formal analysis, Funding acquisition, Investigation, Methodology, Project administration, Resources, Supervision, Validation, Writing – original draft, Writing – review & editing.

Declaration of competing interest

The authors declare that they have no known competing financial interests or personal relationships that could appear to influence the work reported in this paper.

Acknowledgments

The financial support of this research by the National Center for Manufacturing Sciences (NCMS) (Award No.: NCMS-CTMA 142060), Ann Arbor, MI, USA, with John Keippala as the project manager and Dr. Theodore Burye as the government representative of the United States Army Combat Capabilities Development Command (DEVCOM) Ground Vehicle Systems Center (GVSC) is gratefully acknowledged. The initial study of the research was also financially supported in part by the North Dakota State University (NDSU) Development Foundation (Award No.: FAR0031220, FAR0035860), NDSU, Fargo, ND, USA. The views and opinions of the authors expressed herein do not necessarily state or reflect those of the United States Government, NCMS, or any agency thereof. Distribution statement granted by the GVSC for public release: Distribution is unlimited (OPSEC #8105).

Nomenclature

ACP 4,4′ -Azobis (4-cyanopentanoic acid)
AEAPMDS *N*-(2-Aminoethyl)-3-aminopropyltrimethoxysilane
AEAPTS *N*-(2-Aminoethyl)-3-aminopropyltrimethoxysilane
AFCs Alkaline fuel cells
AHAPS *N*-(6-Aminohexyl)-3-aminopropyltrimethoxysilane
AIBN 2,2-Azobisisobutyronitrile
AIT Amine functionalized iron titanate
APTES 3-Aminopropyltriethoxysilane
APTMS 3-Aminopropyltrimethoxysilane
ATRP Atom transfer radical polymerization
BIBr α-bromoisobutyryl bromide
CeO_2 Cerium dioxide
CMDT Cyanomethyl dodecyl trithiocarbonate
CNT Carbon nanotube
CPC 2-Chloropropionyl chloride
CPDB 4-Cyanopentanic acid dithiobenzoate
CPMS 4-Chloromethyl phenyl trimethoxysilane
CRP Controlled radical polymerization
DMFCs Direct methanol fuel cells
DEFCs Direct ethanol fuel cells
DS Degree of sulfonation
E-SN Exfoliated silica nanosheets
GDL Gas diffusion layer
GPTMS (3-Glycidyloxypropyl) trimethoxy silane
HOFCs Hydrogen-oxygen fuel cells
HPSS Hollow P(MAA-co-DVB-co-CMSt)-g-PSt-SO_3H microspheres
IEC Ion exchange capacity
IT-PEMFCs Intermediate temperature proton exchange membrane fuel cells
LAMS Long chain amine modified silica
LT-PEMFCs Low-temperature proton exchange membrane fuel cells
MCFCs Molten carbonate fuel cells
MeO-AMVN Azobis(4 methoxy-2,4-dimethylvaleronitrile)
MOFs Metal organic frameworks
MPS 3-(Methacryloxy)propyltrimethoxysilane
MPTMS 3-Mercaptopropyltrimethoxysilane
NMP Nitroxide-mediated radical polymerization
NP Nanoparticle
NPG Non-precious group
OPBI Poly (4,4′-diphenylether-5,5′- bibenzimidazole)
P(MAA-co-DVB-co-CMSt) Poly (methacrylic acid-*co*-divinylbenzene-*co*-4- chloromethyl styrene)
PA Phosphoric acid
PAA Polyacrylic acid
PAFCs Phosphoric acid fuel cells
PAMPS Poly (2-acrylamido-2- methyl-1-propane sulfonic acid)
PBI Polybenzimidazole
PBI-OO Poly-[(1-(4,4′-diphenylether) − 5 oxybenzimidazole)-benzimidazole]
PC Proton conductivity
PD Power density
PEMFCs Proton exchange membrane fuel cells
PEMs Proton exchange membranes
PES Polyether sulfone
PES-PVP Polyether sulfone-Polyvinylpyrrolidone
PFSA Perfluoro sulfonic acids
PIC Polymer-inorganic composite
PNVI Poly (*N*-vinyl imidazole)
PNVI Poly (*N*-vinyl imidazole)
PNVT Poly (*N*-vinyl-1,2,4-triazole)
Poly (MeOEGMA) Poly (monomethoxy oligo ethylene glycol methacrylate)
PSPM Poly (3-sulfopropylmethacrylate)
PSS Polystyrene sulfonate
PSSA Poly (styrene sulfonic acid)
PSU Polysulfone
PVBP Poly (diethyl vinyl benzyl phosphonate)
PVDF-co-CTFE Poly (vinylidene fluoride-*co*-chlorotrifluoroethylene)
PVImBr Poly (vinylimidazolium) bromide
PVPA Poly (vinylphosphonic acid)
RAFT Reversible addition fragmentation chain transfer polymerization
RCTP Reversible chain transfer polymerization
RH Relative humidity
SI-ATRP Surface initiated atom transfer radical polymerization
SiO_2 Silicon dioxide
ZrO_2 Zirconium dioxide
SN Silica nanosheets
SOFCs Solid oxide fuel cells
SPAEK Sulfonated poly (arylene ether ketone)
SPAES Sulfonated poly (arylene ether sulfone)
sPBI Sulfonated polybenzimidazole
SPEEK Sulfonated ether ether ketone
***S*–TiO_2** Sulfonated titanium dioxide

TEA Triethylamine
TEOS Tetraethoxysilane
TiO_2 Titanium dioxide
TMSPDT *N*-(3-trimethoxysilylpropyl) diethylenetriamine
VImBr Vinyl imidazolium bromide

References

[1] J.M. Andújar, F. Segura, Fuel cells: history and updating. A walk along two centuries, Renew. Sustain. Energy Rev. 13 (9) (Dec. 2009) 2309–2322, https://doi.org/10.1016/j.rser.2009.03.015.

[2] J. Lu, S. Lu, S.P. Jiang, Highly ordered mesoporous Nafion membranes for fuel cells, Chem. Commun. 47 (11) (2011) 3216–3218, https://doi.org/10.1039/c0cc05560c.

[3] M. Winter, R.J. Brodd, What are batteries, fuel cells, and supercapacitors? Chem. Rev. 104 (10) (Oct. 2004) 4245–4269, https://doi.org/10.1021/cr020730k.

[4] S.Ü. Çelik, A. Bozkurt, S.S. Hosseini, Alternatives toward proton conductive anhydrous membranes for fuel cells: heterocyclic protogenic solvents comprising polymer electrolytes, Prog. Polym. Sci. 37 (9) (Sep. 2012) 1265–1291, https://doi.org/10.1016/j.progpolymsci.2011.11.006.

[5] E. Bakangura, L. Wu, L. Ge, Z. Yang, T. Xu, Mixed matrix proton exchange membranes for fuel cells: state of the art and perspectives, Prog. Polym. Sci. 57 (Jun. 2016) 103–152, https://doi.org/10.1016/j.progpolymsci.2015.11.004.

[6] A. Hamnett, Mechanism and electrocatalysis in the direct methanol fuel cell, Catal. Today 38 (4) (Nov. 1997) 445–457, https://doi.org/10.1016/S0920-5861(97)00054-0.

[7] M.A.F. Akhairi, S.K. Kamarudin, Catalysts in direct ethanol fuel cell (DEFC): an overview, Int. J. Hydrogen Energy 41 (7) (Feb. 2016) 4214–4228, https://doi.org/10.1016/j.ijhydene.2015.12.145.

[8] R.-A. Felseghi, E. Carcadea, M.S. Raboaca, C.N. Trufin, C. Filote, Hydrogen fuel cell technology for the sustainable future of stationary applications, Energies 12 (23) (Dec. 2019) 4593, https://doi.org/10.3390/en12234593.

[9] F. Ramadhani, M.A. Hussain, H. Mokhlis, A comprehensive review and technical guideline for optimal design and operations of fuel cell-based cogeneration systems, Processes 7 (12) (Dec. 2019) 950, https://doi.org/10.3390/pr7120950.

[10] S.J. Peighambardoust, S. Rowshanzamir, M. Amjadi, Review of the proton exchange membranes for fuel cell applications, Int. J. Hydrogen Energy 35 (17) (Sep. 2010) 9349–9384, https://doi.org/10.1016/j.ijhydene.2010.05.017.

[11] R. O'Hayre, S. Cha, W. Colella, F.B. Prinz, Fuel Cell Fundamentals, Wiley, 2016, https://doi.org/10.1002/9781119191766.

[12] F. He, et al., High-performance proton-conducting fuel cell with B-site-deficient perovskites for all cell components, Energy Fuels 34 (9) (Sep. 2020) 11464–11471, https://doi.org/10.1021/acs.energyfuels.0c02370.

[13] S.J. Hamrock, A.M. Herring, Proton exchange membrane fuel cells: high-temperature, low-humidity operation, in: Fuel Cells and Hydrogen Production, New York, NY: Springer New York, 2019, pp. 455–476, https://doi.org/10.1007/978-1-4939-7789-5_155.

[14] A.Z. Weber, J. Newman, Modeling transport in polymer-electrolyte fuel cells, Chem. Rev. 104 (10) (Oct. 2004) 4679–4726, https://doi.org/10.1021/cr020729l.

[15] T.V. Nguyen, R.E. White, A water and heat management model for proton-exchange-membrane fuel Cells, J. Electrochem. Soc. 140 (8) (Aug. 1993) 2178–2186, https://doi.org/10.1149/1.2220792.

[16] D. Kim, H. Sohn, S. Kim, A. Lee, J. Lee, Star-shaped polymers having side chain poss groups for solid polymer electrolytes; synthesis, thermal behavior, dimensional stability, and ionic conductivity, J. Polym. Sci. Part A Polym. Chem. 50 (17) (Sep. 2012) 3618–3627, https://doi.org/10.1002/pola.26151.

[17] O. Zholobko, J. Hurley, X.-F. Wu, T. Aulich, J. Thakare, Intermediate-temperature proton exchange membranes based on cerium ultraphosphate composited with polybenzimidazole, J. Electrochem. Soc. 169 (9) (Sep. 2022) 94505, https://doi.org/10.1149/1945-7111/ac90f0.

[18] R. Souzy, B. Ameduri, Functional fluoropolymers for fuel cell membranes, Prog. Polym. Sci. 30 (6) (Jun. 2005) 644–687, https://doi.org/10.1016/j.progpolymsci.2005.03.004.

[19] M.B. Karimi, F. Mohammadi, K. Hooshyari, Recent approaches to improve Nafion performance for fuel cell applications: a review, Int. J. Hydrogen Energy 44 (54) (Nov. 2019) 28919–28938, https://doi.org/10.1016/j.ijhydene.2019.09.096.

[20] Y. Wang, D.F. Ruiz Diaz, K.S. Chen, Z. Wang, X.C. Adroher, Materials, technological status, and fundamentals of PEM fuel cells – a review, Mater. Today 32 (Jan. 2020) 178–203, https://doi.org/10.1016/j.mattod.2019.06.005.

[21] Q. Li, R. He, J.O. Jensen, N.J. Bjerrum, Approaches and recent development of polymer electrolyte membranes for fuel cells operating above 100 °C, Chem. Mater. 15 (26) (Dec. 2003) 4896–4915, https://doi.org/10.1021/cm0310519.

[22] Q. Li, R. He, J.-A. Gao, J.O. Jensen, N.J. Bjerrum, The CO poisoning effect in PEMFCs operational at temperatures up to 200°C, J. Electrochem. Soc. 150 (12) (2003) A1599, https://doi.org/10.1149/1.1619984.

[23] Z. Mossayebi, T. Sariri chi, S. Rowshanzamir, M.J. Parnian, Investigation and optimization of physicochemical properties of sulfated zirconia/sulfonated poly (ether ether ketone) nanocomposite membranes for medium temperature proton exchange membrane fuel cells, Int. J. Hydrogen Energy 41 (28) (Jul. 2016) 12293–12306, https://doi.org/10.1016/j.ijhydene.2016.05.017.

[24] C. Simari, E. Lufrano, A. Brunetti, G. Barbieri, I. Nicotera, Highly-performing and low-cost nanostructured membranes based on polysulfone and layered doubled hydroxide for high-temperature proton exchange membrane fuel cells, J. Power Sources 471 (Sep. 2020) 228440, https://doi.org/10.1016/j.jpowsour.2020.228440.

[25] S. Swier, V. Ramani, J. Fenton, H. Kunz, M. Shaw, R. Weiss, Polymer blends based on sulfonated poly(ether ketone ketone) and poly(ether sulfone) as proton exchange membranes for fuel cells, J. Membr. Sci. (Apr. 2005), https://doi.org/10.1016/j.memsci.2005.02.013.

[26] H. Ko, M. Kim, S.Y. Nam, K. Kim, Research of cross-linked hydrocarbon based polymer electrolyte membranes for polymer electrolyte membrane fuel cell applications, Membrane J. 30 (6) (Dec. 2020) 395–408, https://doi.org/10.14579/MEMBRANE_JOURNAL.2020.30.6.395.

[27] M. Kim, H. Ko, S.Y. Nam, K. Kim, Study on control of polymeric architecture of sulfonated hydrocarbon-based polymers for high-performance polymer electrolyte membranes in fuel cell applications, Polymers 13 (20) (Oct. 2021) 3520, https://doi.org/10.3390/polym13203520.

[28] Z. Huang, B. Lv, L. Zhou, Tao wei, X. Qin, Z. Shao, Ultra-thin h-BN doped high sulfonation sulfonated poly (ether-ether-ketone) of PTFE-reinforced proton exchange membrane, J. Membr. Sci. 644 (Feb. 2022) 120099, https://doi.org/10.1016/j.memsci.2021.120099.

[29] X. Meng, et al., Effect of covalent organic frameworks containing different groups on properties of sulfonated poly(ether ether ketone) matrix proton exchange membranes, Nanomaterials 12 (19) (Oct. 2022) 3518, https://doi.org/10.3390/nano12193518.

[30] K. Kang, D. Kim, Pendant dual-sulfonated poly(arylene ether ketone) multi-block copolymer membranes for enhanced proton conductivity at reduced water swelling, J. Membr. Sci. 578 (May 2019) 103–110, https://doi.org/10.1016/j.memsci.2019.02.043.

[31] T. Holmes, T.J.G. Skalski, M. Adamski, S. Holdcroft, Stability of hydrocarbon fuel cell membranes: reaction of hydroxyl radicals with sulfonated phenylated polyphenylenes, Chem. Mater. 31 (4) (Feb. 2019) 1441–1449, https://doi.org/10.1021/acs.chemmater.8b05302.

[32] N.R. Kang, T.H. Pham, P. Jannasch, Polyaromatic perfluorophenylsulfonic acids with high radical resistance and proton conductivity, ACS Macro Lett. 8 (10) (Oct. 2019) 1247–1251, https://doi.org/10.1021/acsmacrolett.9b00615.

[33] G. Ye, K. Li, C. Xiao, W. Chen, H. Zhang, M. Pan, Nafion ® —titania nanocomposite proton exchange membranes, J. Appl. Polym. Sci. 120 (2) (Apr. 2011) 1186–1192, https://doi.org/10.1002/app.33031.

[34] H. Ranganathan, M. Vinothkannan, A.R. Kim, V. Subramanian, M. Oh, D.J. Yoo, Simultaneous improvement of power density and durability of sulfonated poly(ether ether ketone) membrane by embedding CeO_2-$ATiO_2$: a comprehensive study in low humidity proton exchange membrane fuel cells, Int. J. Energy Res. 46 (7) (Jun. 2022) 9041–9057, https://doi.org/10.1002/er.7781.

[35] K.H. Lee, J.Y. Chu, A.R. Kim, D.J. Yoo, Effect of functionalized SiO_2 toward proton conductivity of composite membranes for PEMFC application, Int. J. Energy Res. 43 (10) (Aug. 2019) 5333–5345, https://doi.org/10.1002/er.4610.

[36] A. Poongan, M. Kesava, A. Mandal, E. Murugan, Effect of ZrO_2 nanoparticles on phosphoric acid-doped poly (ethylene imine)/polyvinyl alcohol) membrane for medium-temperature polymer electrolyte membrane fuel cell applications, Int. J. Hydrogen Energy 48 (70) (Aug. 2023) 27371–27382, https://doi.org/10.1016/j.ijhydene.2023.03.418.

[37] Y. Ou, et al., Chitosan-based composite membranes containing chitosan-coated carbon nanotubes for polymer electrolyte membranes, Polym. Adv. Technol. 29 (1) (Jan. 2018) 612–622, https://doi.org/10.1002/pat.4171.

[38] A.K. Sahu, K. Ketpang, S. Shanmugam, O. Kwon, S. Lee, H. Kim, Sulfonated graphene–Nafion composite membranes for polymer electrolyte fuel cells operating under reduced relative humidity, J. Phys. Chem. C 120 (29) (Jul. 2016) 15855–15866, https://doi.org/10.1021/acs.jpcc.5b11674.

[39] J. Ren, et al., Long-term durable anion exchange membranes based on imidazole-functionalized poly(ether ether ketone) incorporating cationic metal−organic framework, Adv. Powder Mater. 1 (2) (Apr. 2022) 100017, https://doi.org/10.1016/j.apmate.2021.11.004.

[40] M.J. Parnian, S. Rowshanzamir, A.K. Prasad, S.G. Advani, High durability sulfonated poly (ether ether ketone)-ceria nanocomposite membranes for proton exchange membrane fuel cell applications, J. Membr. Sci. 556 (Jun. 2018) 12–22, https://doi.org/10.1016/j.memsci.2018.03.083.

[41] H. Pu, L. Liu, Z. Chang, J. Yuan, Organic/inorganic composite membranes based on polybenzimidazole and nano-SiO_2, Electrochim. Acta 54 (28) (Dec. 2009) 7536–7541, https://doi.org/10.1016/j.electacta.2009.08.011.

[42] N.N. Krishnan, et al., Polybenzimidazole (PBI-OO) based composite membranes using sulfophenylated TiO_2 as both filler and crosslinker, and their use in the HT-PEM fuel cell, J. Membr. Sci. 560 (Aug. 2018) 11–20, https://doi.org/10.1016/j.memsci.2018.05.006.

[43] J. Lobato, P. Cañizares, M.A. Rodrigo, D. Úbeda, F.J. Pinar, A novel titanium PBI-based composite membrane for high temperature PEMFCs, J. Membr. Sci. 369 (1–2) (Mar. 2011) 105–111, https://doi.org/10.1016/j.memsci.2010.11.051.

[44] M. Moradi, A. Moheb, M. Javanbakht, K. Hooshyari, Experimental study and modeling of proton conductivity of phosphoric acid doped PBI-Fe_2TiO_5 nanocomposite membranes for using in high temperature proton exchange membrane fuel cell (HT-PEMFC), Int. J. Hydrogen Energy 41 (4) (Jan. 2016) 2896–2910, https://doi.org/10.1016/j.ijhydene.2015.12.100.

[45] M.M. Hasani-Sadrabadi, E. Dashtimoghadam, F.S. Majedi, H. Moaddel, A. Bertsch, P. Renaud, Superacid-doped polybenzimidazole-decorated carbon nanotubes: a novel high-performance proton exchange nanocomposite membrane, Nanoscale 5 (23) (2013) 11710, https://doi.org/10.1039/c3nr02886k.

[46] H. Wu, W. Hou, J. Wang, L. Xiao, Z. Jiang, Preparation and properties of hybrid direct methanol fuel cell membranes by embedding organophosphorylated titania

submicrospheres into a chitosan polymer matrix, J. Power Sources 195 (13) (Jul. 2010) 4104–4113, https://doi.org/10.1016/j.jpowsour.2010.01.079.
[47] R.R. Abbaraju, N. Dasgupta, A.V. Virkar, Composite Nafion membranes containing nanosize TiO_2/SnO_2 for proton exchange membrane fuel cells, J. Electrochem. Soc. 155 (12) (2008) B1307, https://doi.org/10.1149/1.2994079.
[48] E. Chalkova, M.V. Fedkin, D.J. Wesolowski, S.N. Lvov, Effect of TiO_2 surface properties on performance of Nafion-based composite membranes in high temperature and low relative humidity PEM fuel cells, J. Electrochem. Soc. 152 (9) (2005) A1742, https://doi.org/10.1149/1.1971216.
[49] Y. Duan, et al., Synergistic Utilization of a CeO_2-anchored bifunctionalized metal–organic framework in a polymer nanocomposite toward achieving high power density and durability of PEMFC, ACS Sustain. Chem. Eng. 11 (13) (Apr. 2023) 5270–5283, https://doi.org/10.1021/acssuschemeng.3c00046.
[50] T.J. Peckham, J. Schmeisser, M. Rodgers, S. Holdcroft, Main-chain, statistically sulfonated proton exchange membranes: the relationships of acid concentration and proton mobility to water content and their effect upon proton conductivity, J. Mater. Chem. 17 (30) (2007) 3255, https://doi.org/10.1039/b702339a.
[51] S. Kango, S. Kalia, A. Celli, J. Njuguna, Y. Habibi, R. Kumar, Surface modification of inorganic nanoparticles for development of organic–inorganic nanocomposites—a review, Prog. Polym. Sci. 38 (8) (Aug. 2013) 1232–1261, https://doi.org/10.1016/j.progpolymsci.2013.02.003.
[52] Y.S. Khoo, W.J. Lau, Y.Y. Liang, M. Karaman, M. Gürsoy, A.F. Ismail, Eco-friendly surface modification approach to develop thin film nanocomposite membrane with improved desalination and antifouling properties, J. Adv. Res. 36 (Feb. 2022) 39–49, https://doi.org/10.1016/j.jare.2021.06.011.
[53] N. Ahmed, et al., Nano-engineering and micromolecular science of polysilsesquioxane materials and their emerging applications, J. Mater. Chem. A 7 (38) (2019) 21577–21604, https://doi.org/10.1039/C9TA04575A.
[54] M. Sypabekova, A. Hagemann, D. Rho, S. Kim, Review: 3-Aminopropyltriethoxysilane (APTES) deposition methods on oxide surfaces in solution and vapor phases for biosensing applications, Biosensors 13 (1) (Dec. 2022) 36, https://doi.org/10.3390/bios13010036.
[55] A. Issa, A. Luyt, Kinetics of alkoxysilanes and organoalkoxysilanes polymerization: a Review, Polymers 11 (3) (Mar. 2019) 537, https://doi.org/10.3390/polym11030537.
[56] P. Salarizadeh, M. Javanbakht, S. Pourmahdian, H. Beydaghi, Influence of amine-functionalized iron titanate as filler for improving conductivity and electrochemical properties of SPEEK nanocomposite membranes, Chem. Eng. J. 299 (Sep. 2016) 320–331, https://doi.org/10.1016/j.cej.2016.04.086.
[57] P. Salarizadeh, M. Javanbakht, S. Pourmahdian, A. Bagheri, H. Beydaghi, M. Enhessari, Surface modification of Fe_2TiO_5 nanoparticles by silane coupling agent: synthesis and application in proton exchange composite membranes, J. Colloid Interface Sci. 472 (Jun. 2016) 135–144, https://doi.org/10.1016/j.jcis.2016.03.036.
[58] Z. Guo, et al., High-performance polymer electrolyte membranes incorporated with 2D silica nanosheets in high-temperature proton exchange membrane fuel cells, J. Energy Chem. 64 (Jan. 2022) 323–334, https://doi.org/10.1016/j.jechem.2021.04.061.
[59] K. Pourzare, M. Zargar, S. Farhadi, M.M. Hassani Sadrabadi, Y. Mansourpanah, Aminosilica-functionalized Co_3O_4 nanostructures in proton exchange mixed matrix membranes for enhanced separation efficiency of direct methanol fuel cells, ACS Appl. Nano Mater. 6 (1) (Jan. 2023) 296–304, https://doi.org/10.1021/acsanm.2c04405.
[60] J. Li, et al., Facilitating proton transport with enhanced water conservation membranes for direct methanol fuel cells, ACS Sustain. Chem. Eng. 8 (15) (Apr. 2020) 5880–5890, https://doi.org/10.1021/acssuschemeng.9b07563.
[61] S. Lee, K. Seo, R.V. Ghorpade, K.-H. Nam, H. Han, High temperature anhydrous proton exchange membranes based on chemically-functionalized titanium/polybenzimidazole composites for fuel cells, Mater. Lett. 263 (Mar. 2020) 127167, https://doi.org/10.1016/j.matlet.2019.127167.
[62] M.A. Imran, T. Li, X. Wu, X. Yan, A.-S. Khan, G. He, Sulfonated polybenzimidazole/amine functionalized titanium dioxide (sPBI/AFT) composite electrolyte membranes for high temperature proton exchange membrane fuel cells usage, Chin. J. Chem. Eng. 28 (9) (Sep. 2020) 2425–2437, https://doi.org/10.1016/j.cjche.2020.05.016.
[63] Y. Jun, H. Zarrin, M. Fowler, Z. Chen, Functionalized titania nanotube composite membranes for high temperature proton exchange membrane fuel cells, Int. J. Hydrogen Energy 36 (10) (May 2011) 6073–6081, https://doi.org/10.1016/j.ijhydene.2011.02.030.
[64] S. Singha, T. Jana, Structure and properties of polybenzimidazole/silica nanocomposite electrolyte membrane: influence of organic/inorganic interface, ACS Appl. Mater. Interfaces 6 (23) (Dec. 2014) 21286–21296, https://doi.org/10.1021/am506260j.
[65] L. Wu, U. Glebe, A. Böker, Surface-initiated controlled radical polymerizations from silica nanoparticles, gold nanocrystals, and bionanoparticles, Polym. Chem. 6 (29) (2015) 5143–5184, https://doi.org/10.1039/C5PY00525F.
[66] D. Yang, M.N.N.L. Oo, G.R. Deen, Z. Li, X.J. Loh, Nano-star-shaped polymers for drug delivery applications, Macromol. Rapid Commun. 38 (21) (Nov. 2017), https://doi.org/10.1002/marc.201700410.
[67] J. Liu, Y. Ye, Y. Xue, X. Xie, Y. Mai, Recent advances in covalent functionalization of carbon nanomaterials with polymers: strategies and perspectives, J. Polym. Sci. Part A Polym. Chem. 55 (4) (Feb. 2017) 622–631, https://doi.org/10.1002/pola.28426.
[68] J.T. Park, J.H. Koh, D.K. Roh, Y.G. Shul, J.H. Kim, Proton-conducting nanocomposite membranes based on P(VDF-co-CTFE)-g-PSSA graft copolymer and TiO_2–PSSA nanoparticles, Int. J. Hydrogen Energy 36 (2) (Jan. 2011) 1820–1827, https://doi.org/10.1016/j.ijhydene.2009.12.168.
[69] A. Farrukh, et al., Polymer brush functionalized SiO_2 nanoparticle based Nafion nanocomposites: a novel avenue to low-humidity proton conducting membranes, Polym. Chem. 6 (31) (2015) 5782–5789, https://doi.org/10.1039/C5PY00514K.
[70] E. Labalme, G. David, P. Buvat, J. Bigarre, T. Boucheteau, New hybrid membranes based on phosphonic acid functionalized silica particles for PEMFC, J. Polym. Sci. Part A Polym. Chem. 50 (7) (Apr. 2012) 1308–1316, https://doi.org/10.1002/pola.25895.
[71] W. Zhang, et al., Enhanced water retention and proton conductivity of proton exchange membranes by incorporating hollow polymer microspheres grafted with sulfonated polystyrene brushes, RSC Adv. 5 (7) (2015) 5343–5356, https://doi.org/10.1039/C4RA13582B.
[72] K.T. Park, et al., Composite membranes based on a sulfonated poly(arylene ether sulfone) and proton-conducting hybrid silica particles for high temperature PEMFCs, Int. J. Hydrogen Energy 36 (17) (Aug. 2011) 10891–10900, https://doi.org/10.1016/j.ijhydene.2011.05.151.
[73] R. Shahabadi, M. Abdollahi, A. Sharif, Preparation, characterization and properties of polymer electrolyte nanocomposite membranes containing silica nanoparticles modified via surface-initiated atom transfer radical polymerization, Int. J. Hydrogen Energy 40 (9) (Mar. 2015) 3749–3761, https://doi.org/10.1016/j.ijhydene.2015.01.090.
[74] J.J. Smith, I. Zharov, Preparation and proton conductivity of sulfonated polymer-modified sintered and Self-assembled silica colloidal crystals, Chem. Mater. 21 (10) (May 2009) 2013–2019, https://doi.org/10.1021/cm8020929.
[75] R. Koyilapu, S. Singha, S.N.R. Kutcherlapati, T. Jana, Grafting of vinylimidazolium-type poly(ionic liquid) on silica nanoparticle through RAFT polymerization for constructing nanocomposite based PEM, Polymer (Guildf). 195 (May 2020) 122458, https://doi.org/10.1016/j.polymer.2020.122458.
[76] K. Tabata, et al., Proton conductivity dependence on the surface polymer thickness of core–shell type nanoparticles in a proton exchange membrane, Nanoscale Adv. 4 (22) (2022) 4714–4723, https://doi.org/10.1039/D2NA00450J.
[77] K. Koseki, et al., Effect of surface silanol density on the proton conductivity of polymer-surface-functionalized silica nanoparticles, ACS Sustain. Chem. Eng. 9 (30) (Aug. 2021) 10093–10099, https://doi.org/10.1021/acssuschemeng.1c01922.
[78] T. Nohara, et al., Core size-dependent proton conductivity of silica filler-functionalized polymer electrolyte membrane, ACS Sustain. Chem. Eng. 8 (39) (Oct. 2020) 14674–14678, https://doi.org/10.1021/acssuschemeng.0c04033.
[79] N. Mukherjee, A. Das, M. Dhara, T. Jana, Surface initiated RAFT polymerization to synthesize N-heterocyclic block copolymer grafted silica nanofillers for improving PEM properties, Polymer (Guildf). 236 (Nov. 2021) 124315, https://doi.org/10.1016/j.polymer.2021.124315.
[80] S.R. Kutcherlapati, R. Koyilapu, T. Jana, Poly(N -vinyl imidazole) grafted silica nanofillers: synthesis by RAFT polymerization and nanocomposites with polybenzimidazole, J. Polym. Sci. Part A Polym. Chem. 56 (4) (Feb. 2018) 365–375, https://doi.org/10.1002/pola.28917.
[81] K. Tabata, et al., Facile-controlling of the coating amount of poly(acrylic acid)- b -polystyrene coated on silica nanoparticles for polymer electrolyte membrane, Jpn. J. Appl. Phys. 59 (SI) (Jun. 2020) SIIH01, https://doi.org/10.35848/1347-4065/ab7476.
[82] K. Shito, J. Matsui, Y. Takahashi, A. Masuhara, T. Arita, Proton conductivity of poly(acrylic acid)- b -polystyrene-coated silica nanoparticles synthesized by reversible addition–fragmentation chain transfer polymerization with particles, Chem. Lett. 47 (1) (Jan. 2018) 9–12, https://doi.org/10.1246/cl.170752.
[83] K. Scott, C. Xu, X. Wu, Intermediate temperature proton-conducting membrane electrolytes for fuel cells, WIREs Energy Environ 3 (1) (Jan. 2014) 24–41, https://doi.org/10.1002/wene.64.
[84] T. Xiao, R. Wang, Z. Chang, Z. Fang, Z. Zhu, C. Xu, Electrolyte membranes for intermediate temperature proton exchange membrane fuel cell, Prog. Nat. Sci. Mater. Int. 30 (6) (Dec. 2020) 743–750, https://doi.org/10.1016/j.pnsc.2020.08.014.
[85] Z. Zhou, O. Zholobko, X.-F. Wu, T. Aulich, J. Thakare, J. Hurley, Polybenzimidazole-based polymer electrolyte membranes for high-temperature fuel cells: current status and prospects, Energies 14 (1) (Dec. 2020) 135, https://doi.org/10.3390/en14010135.
[86] T.R. Aulich, J. Thakare, J. Hurley, X. Wu, Z. Zhou, O. Zholobko, Proton-exchange membrane. US Patent No. 20210009775, 2021.
[87] T. Søndergaard, et al., Long-term durability of HT-PEM fuel cells based on thermally cross-linked polybenzimidazole, J. Power Sources 342 (Feb. 2017) 570–578, https://doi.org/10.1016/j.jpowsour.2016.12.075.
[88] J.H. Liao, et al., Oxidative degradation of polybenzimidazole membranes as electrolytes for high temperature proton exchange membrane fuel cells, Fuel Cell. 11 (6) (Dec. 2011) 745–755, https://doi.org/10.1002/fuce.201000146.
[89] Y. Oono, A. Sounai, M. Hori, Long-term cell degradation mechanism in high-temperature proton exchange membrane fuel cells, J. Power Sources 210 (Jul. 2012) 366–373, https://doi.org/10.1016/j.jpowsour.2012.02.098.
[90] P. Mustarelli, E. Quartarone, S. Grandi, A. Carollo, A. Magistris, Polybenzimidazole-based membranes as a real alternative to Nafion for fuel cells operating at low temperature, Adv. Mater. 20 (7) (Apr. 2008) 1339–1343, https://doi.org/10.1002/adma.200701767.
[91] A.A. Lysova, I.I. Ponomarev, A.B. Yaroslavtsev, Composite materials based on polybenzimidazole and inorganic oxides, Solid State Ionics 188 (1) (Apr. 2011) 132–134, https://doi.org/10.1016/j.ssi.2010.10.010.
[92] J. Lobato, P. Cañizares, M.A. Rodrigo, D. Úbeda, F.J. Pinar, Enhancement of the fuel cell performance of a high temperature proton exchange membrane fuel cell

running with titanium composite polybenzimidazole-based membranes, J. Power Sources 196 (20) (Oct. 2011) 8265–8271, https://doi.org/10.1016/j.jpowsour.2011.06.011.
[93] F.J. Pinar, P. Cañizares, M.A. Rodrigo, D. Ubeda, J. Lobato, Titanium composite PBI-based membranes for high temperature polymer electrolyte membrane fuel cells. Effect on titanium dioxide amount, RSC Adv. 2 (4) (2012) 1547–1556, https://doi.org/10.1039/C1RA01084K.
[94] J. Hao, Y. Jiang, X. Gao, F. Xie, Z. Shao, B. Yi, Degradation reduction of polybenzimidazole membrane blended with CeO_2 as a regenerative free radical scavenger, J. Membr. Sci. 522 (Jan. 2017) 23–30, https://doi.org/10.1016/j.memsci.2016.09.010.
[95] T. Okuhara, Water-tolerant solid acid catalysts, Chem. Rev. 102 (10) (Oct. 2002) 3641–3666, https://doi.org/10.1021/cr0103569.
[96] P. Gómez-Romero, J.A. Asensio, S. Borrós, Hybrid proton-conducting membranes for polymer electrolyte fuel cells, Electrochim. Acta 50 (24) (Aug. 2005) 4715–4720, https://doi.org/10.1016/j.electacta.2005.02.029.
[97] R. He, Proton conductivity of phosphoric acid doped polybenzimidazole and its composites with inorganic proton conductors, J. Membr. Sci. 226 (1–2) (Dec. 2003) 169–184, https://doi.org/10.1016/j.memsci.2003.09.002.
[98] P. Staiti, M. Minutoli, Influence of composition and acid treatment on proton conduction of composite polybenzimidazole membranes, J. Power Sources 94 (1) (Feb. 2001) 9–13, https://doi.org/10.1016/S0378-7753(00)00597-8.
[99] Y.S. Kim, F. Wang, M. Hickner, T.A. Zawodzinski, J.E. McGrath, Fabrication and characterization of heteropolyacid ($H_3PW_{12}O_{40}$)/directly polymerized sulfonated poly(arylene ether sulfone) copolymer composite membranes for higher temperature fuel cell applications, J. Membr. Sci. 212 (1–2) (Feb. 2003) 263–282, https://doi.org/10.1016/S0376-7388(02)00507-0.
[100] R.K. Gover, N.D. Withers, S. Allen, R.L. Withers, J.S.O. Evans, Structure and phase transitions of SnP_2O_7, J. Solid State Chem. 166 (1) (Jun. 2002) 42–48, https://doi.org/10.1006/jssc.2002.9554.
[101] M. Behm, Influence of structure and composition upon performance of tin phosphate based negative electrodes for lithium batteries, Electrochim. Acta 47 (11) (Mar. 2002) 1727–1738, https://doi.org/10.1016/S0013-4686(02)00017-8.
[102] M. Nagao, T. Kamiya, P. Heo, A. Tomita, T. Hibino, M. Sano, Proton conduction in In^{3+}-doped SnP_2O_7 at intermediate temperatures, J. Electrochem. Soc. 153 (8) (2006) A1604, https://doi.org/10.1149/1.2210669.
[103] P. Heo, M. Nagao, M. Sano, T. Hibino, A high performance Pt-free anode for intermediate-temperature fuel cells, ECS Trans. 3 (1) (Oct. 2006) 453–458, https://doi.org/10.1149/1.2356166.
[104] P. Heo, M. Nagao, M. Sano, T. Hibino, A High-performance Mo_2C-ZrO_2 anode catalyst for intermediate-temperature fuel cells, J. Electrochem. Soc. 154 (1) (2007) B53, https://doi.org/10.1149/1.2382268.
[105] M. Nagao, T. Kamiya, P. Heo, T. Hibino, M. Sano, A. Tomita, Proton conduction in In^{3+}-doped SnP_2O_7 with various P/(Sn+In) ratios, ECS Trans. 2 (10) (Feb. 2007) 43–49, https://doi.org/10.1149/1.2408942.
[106] P. Heo, M. Nagao, T. Kamiya, M. Sano, A. Tomita, T. Hibino, $Sn_{0.9}In_{0.1}P_2O_7$-based organic/inorganic composite membranes, J. Electrochem. Soc. 154 (1) (2007) B63, https://doi.org/10.1149/1.2388737.
[107] T.V. Anfimova, Metal phosphates as proton conducting materials for intermediate temperature fuel cell and electrolyser applications (PhD Thesis), Technical University of Denmark, Denmark, 2014.
[108] O. Zholobko, X. Wu, Z. Zhou, T. Aulich, J. Thakare, J. Hurley, A comparative experimental study of the hygroscopic and mechanical behaviors of electrospun nanofiber membranes and solution-cast films of polybenzimidazole, J. Appl. Polym. Sci. 137 (39) (Oct. 2020), https://doi.org/10.1002/app.49639.
[109] J. Smith, D. Bedrov, Smith, A molecular dynamics simulation study of nanoparticle interactions in a model polymer-nanoparticle composite, Compos. Sci. Technol. 63 (11) (Aug. 2003) 1599–1605, https://doi.org/10.1016/S0266-3538(03)00061-7.
[110] V. Ganesan, C.J. Ellison, V. Pryamitsyn, Mean-field models of structure and dispersion of polymer-nanoparticle mixtures, Soft Matter 6 (17) (2010) 4010, https://doi.org/10.1039/b926992d.
[111] D. Meng, S.K. Kumar, J.M.D. Lane, G.S. Grest, Effective interactions between grafted nanoparticles in a polymer matrix, Soft Matter 8 (18) (2012) 5002, https://doi.org/10.1039/c2sm07395a.
[112] L.F.A. Bernardo, A.P.B.M. Amaro, D.G. Pinto, S.M.R. Lopes, Modeling and simulation techniques for polymer nanoparticle composites - A review, Comput. Mater. Sci. 118 (2016) 32–46, https://doi.org/10.1016/j.commatsci.2016.02.025.
[113] P. Khan, R. Kaushik, A. Jayaraj, Approaches and perspective of coarse-grained modeling and simulation for polymer-nanoparticle hybrid systems, ACS Omega 7 (51) (2022) 47567–47586, https://doi.org/10.1021/acsomega.2c06248.
[114] P. Choi, N.H. Jalani, R. Datta, Thermodynamics and proton transport in Nafion, J. Electrochem. Soc. 152 (3) (2005) E123, https://doi.org/10.1149/1.1859814.
[115] P. Choi, N.H. Jalani, R. Datta, Thermodynamics and proton transport in Nafion III. Proton transport in Nafion/sulfated ZrO_2 nanocomposite membranes, J. Electrochem. Soc. 152 (8) (2005), https://doi.org/10.1149/1.1945668.
[116] P.B. Balbuena, E.J. Lamas, Y. Wang, Molecular modeling studies of polymer electrolytes for power sources, Electrochim. Acta 50 (19) (Jun. 2005) 3788–3795, https://doi.org/10.1016/j.electacta.2005.02.063.
[117] M. Rahmati, M. Jangali, Molecular dynamics simulation of proton conductivity enhancement in polymer membranes by Y-doped $BaCeO_3$ nanoparticles, Comput. Mater. Sci. 169 (Nov. 2019) 109139, https://doi.org/10.1016/j.commatsci.2019.109139.
[118] M. Wagner, et al., Mechanism of ion conductivity through polymer-stabilized CsH_2PO_4 nanoparticular layers from experiment and theory, J. Mater. Chem. A 7 (48) (2019) 27367–27376, https://doi.org/10.1039/C9TA04275J.
[119] A. Shirdast, A. Sharif, M. Abdollahi, Prediction of proton conductivity of graphene oxide-containing polymeric membranes, Int. J. Hydrogen Energy 39 (4) (Jan. 2014) 1760–1768, https://doi.org/10.1016/j.ijhydene.2013.11.046.
[120] De Angelis, G.C. Sarti, Gas sorption and permeation in mixed matrix membranes based on glassy polymers and silica nanoparticles, Curr. Opin. Chem. Eng. 1 (2) (May 2012) 148–155, https://doi.org/10.1016/j.coche.2012.02.007.
[121] D.J. Kim, M.J. Jo, S.Y. Nam, A review of polymer–nanocomposite electrolyte membranes for fuel cell application, J. Ind. Eng. Chem. 21 (Jan. 2015) 36–52, https://doi.org/10.1016/j.jiec.2014.04.030.
[122] H. Wu, M. Zamanian, B. Kruczek, J. Thibault, Gas permeation model of mixed-matrix membranes with embedded impermeable cuboid nanoparticles, Membranes (Basel). 10 (12) (2020) 1–20, https://doi.org/10.3390/membranes10120422.
[123] M. Porozhnyy, P. Huguet, M. Cretin, E. Safronova, V. Nikonenko, Mathematical modeling of transport properties of proton-exchange membranes containing immobilized nanoparticles, Int. J. Hydrogen Energy 41 (34) (Sep. 2016) 15605–15614, https://doi.org/10.1016/j.ijhydene.2016.06.057.
[124] S. Nemat-Nasser, M. Hori, Micromechanics : overall properties of heterogeneous materials, 2nd Ed.),", North-Holland, Amsterdam, The Netherlands, 1999.
[125] M. Wang, N. Pan, Predictions of effective physical properties of complex multiphase materials, Mater. Sci. Eng. R Reports 63 (1) (Dec. 2008) 1–30, https://doi.org/10.1016/j.mser.2008.07.001.
[126] K. Pietrak, T.S. Wiśniewski, A review of models for effective thermal conductivity of composite materials, 2015.